Coaxial electrospinning for the reinforcement of nanofibre mats

By

Renier Kemp

Dissertation presented in partial fulfilment of the requirements for the degree of Master of Science

at

Stellenbosch University

Department of Chemistry and Polymer Science

Faculty of Natural Sciences

Promoter: Dr N. P. Gule

Co-promoter: Prof. L. Klumperman

March 2017

Declaration

By submitting this thesis electronically, I declare that the entirety of the work contained therein is my own, original work, that I am the sole author thereof (save to the extent explicitly otherwise stated), that reproduction and publication thereof by Stellenbosch University will not infringe any third party rights and that I have not previously in its entirety or in part submitted it for obtaining any qualification.

March 2017

Abstract

Styrene -*N*-(*N'*,*N'*-dimethyl-3-aminopropyl)maleimide copolymer (SMI-P) was prepared by treating styrene-maleic anhydride copolymer (SMA) with *N*,*N*-dimethyl-3-aminopropylamine (DMAPA). The SMI-P copolymer was fully characterized with Fourier Transform Infrared Spectroscopy (FTIR), Differential Scanning Calorimetry (DSC) and Nuclear Magnetic Resonance (NMR) spectroscopy. Thereafter the polymer was co-electrospun with nylon 6 to produce fibres with core-shell morphology. The core-shell morphology was expected to provide a stronger fibre system for application in water filtration. Core-shell fibres of poly(styrene-*co*-N-(*N'*,*N'*-dimethyl-3-aminopropyl) maleimide) (SMI-P) (shell) and nylon 6 (core) were produced through the coaxial electrospinning technique. The fabricated fibres were characterized using Scanning Electron Microscopy (SEM), Scanning Transmission Electron Microscopy (STEM) and Confocal Microscopy (CM) to provide evidence of the core-shell structure formation. Dissolution tests were also carried out in order to provide further certainty that the core-shell morphology was formed. The dip coating technique was evaluated as a second route towards the formation of coaxial fibres. Mechanical tests were performed on both the core-shell fibres and the coated fibres as well as pristine SMI-P fibres to confirm reinforcement of the fibre mats. Antimicrobial tests were performed on the fabricated fibres via two techniques namely the diffusion disc and live/dead fluorescence methods. Both methods were performed on the samples to determine if the SMI-P retained its antimicrobial activity even after fibre reinforcement. The fibres were found to be potent against *Staphylococcus aureus, Salmonella typhi, Pseudomonas aeruginosa, Escherichia coli,* methicillin-resistant *Staphylococcus aureus,* and *Bacillus subtilis.*

Opsomming

Stireen-N-(N', N'-dimetiel-3-aminopropiel) maleimiedkopolimeer (SMI-P) is voorberei deur die behandeling van stireen-maleïen anhidriedkopolimeer (SMA) met N,N-dimetiel-3-aminopropielamien (DMAPA). Die SMI-P kopolimeer is ten volle gekaraktiseer met behulp van Fourier-transform infrarooispektroskopie (FTIR), differensiële skandeerkalorimetrie (DSK) en kernmagnetiese resonansie (KMR). Daarna is die polimeer ge-elektrospin met nylon 6 om nanovesels met 'n kern-skilmorfologie te maak. Daar is verwag dat die kern-skilmorfologie n sterker veselstelsel sou voortbring vir die toepassing in waterfiltrasie. Kern-skilvesel van poli(stireen-N-(N',N'-dimetiel-3-aminopropiel) maleimiedkopolimeer (SMI-P) (skil) en nylon 6 (kern) is voorberei met die koaksiale elektrospintegniek. Die vervaardigde vesel is gekarakteriseer met behulp van skandeerelektronmikroskopie (SEM), skanderingstransmissie elektronmikroskopie (STEM) en konfokale mikroskopie (KM) om bewys te lewer van die kern-skil struktuurvorming . Ontbindingstoetse is ook gedoen om verder te bewys dat die kern-skilmorfologie bereik is. Die dompellaagtegniek is geëvalueer as 'n tweede roete vir die vorming van koaksiale nanovesels. Meganiese toetse is uitgevoer op die kern-skilvesel en die bedekte vesel, asook ongerepte SMI-P vesel om die versterking van die veselmatte te bevestig. Antimikrobiese toetse is uitgevoer op die voorbereide nanovesels deur twee tegnieke, naamlik die sone inhibisie en lewende/dooie fluoressensie metodes, te gebruik. Beide metodes is uitgevoer op die monsters om te bepaal of die SMI-P sy antimikrobiese aktiwiteit na veselversterking behou. . Daar is bevind dat die vesels aktief is teen *Staphylococcus aureus, Salmonella typhi, Pseudomonas aeruginosa, Escherichia coli,* metisillienweerstandige *Staphylococcus aureus,* asook *Bacillus subtilis.*

Acknowledgements

I would like to sincerely thank the following people who contributed towards the completion of this project:

- My supervisors Dr Gule and Prof. Klumperman for giving me the opportunity to conduct this study under their leadership. Their knowledge and experience made it an honour to study under them.
- To my family for all their support and reassurances which pushed me and helped in the completion of this project.
- My friends for their assistance when things got tough and helped me push through to the end.
- The Free Radical group for all their assistance and support.
- The Central Analytical Facilities staff who helped in the analysis on my samples.
- The National Research Foundation for funding.

Table of Contents

List of Figures

List of Tables

List of Abbreviations

Differential Scanning Calorimetry (DSC)

Extra-High Tension (EHT)

Fourier Transform Infrared Spectroscopy (FTIR)

Luria Bertani Broth (LB)

Maleic anhydride (MA)

N,N-dimethyl-3-aminopropylamine (DMAPA)

N,N-dimethylformamide (DMF)

Nuclear Magnetic Resonance (NMR)

Scanning Electron (SE)

Scanning Electron Microscopy (SEM)

Scanning Transmission Electron Microscopy (STEM)

Styrene-maleic anhydride copolymer (SMA)

Styrene-*N*-(*N'*,*N'*-dimethyl-3-aminopropyl)maleimide copolymer (SMI-P)

Tetrahydrofuran (THF)

Thermally-induced (TIPS)

Transmission Electron Microscope (TEM)

Vapour-induced (VIPS)

Working distance (WD)

Confocal Microscopy (CM)

CHAPTER 1

Introduction

1.1   Introduction

A sixth of the world's population does not have access to safe drinking water.[1] Drinking water resources are being strained due to the increasing world population and many countries around the world are looking into water reuse to augment their water supplies. The use of nanofiltration is an effective way to remove pathogens through the incorporation of antimicrobial and antiviral components in their system.[2-3] Nanofiltration systems have advantages over conventional systems. These include low basis weight (ease in transportation), high permeability and with their small pore sizes. The advantage of these small pore sizes are suitable in the removal of unwanted particles that are in the nanometre range unlike conventional systems that only remove unwanted particles in the micrometre range.[4-5]

The Klumperman group at Stellenbosch University patented antimicrobial poly(styrene-*co-N-(N',N'*-dimethyl-3-aminopropyl)maleimide) (SMI-P) nanofibres in 2011. These fibres are potent against a wide range of bacteria.[6-7] A drawback to the application of these fibres in filtration applications was the poor mechanical properties of the fibres. [8]

The aim of this project was to harness the excellent antimicrobial properties exhibited by SMI-P fibres and improve the mechanical properties of nanofibres with the application in water filtration systems. Nylon 6 was chosen as a strengthening polymer because of its high tensile strength and high abrasion resistance. Two different methods were used to reinforce the fibres, namely coaxial electrospinning and a coating process. The coaxial method would allow for the SMI-P nanofibres to have a nylon 6 core inside, which would increase the tensile strength of the fibres. The coating process would use already spun nylon 6 fibres and then coat these fibres with SMI-P, which would give the strength needed and allow the fibres to have the antimicrobial properties.

1.2   Motivation

The Klumperman group at Stellenbosch University successfully fabricated antimicrobial SMI-P nanofibres in 2011.[8] These fibres were tested against several bacteria strains and were found to have a wide-spectrum of antimicrobial activity. Further tests on these fibres however showed that the fibres were very brittle thus limiting their applications. Due to the exceptional antimicrobial properties, these fibres were considered as possibly good candidates for the use in water filtration systems. The fibres were however too brittle to withstand filtration pressures. Thus, the main aim of this research project was to strengthen the SMI-P nanofibres without losing any of the antimicrobial properties.

Coaxial electrospinning is a modification of the traditional electrospinning technique, which allows for a one step encapsulation of different materials and the electrospinning of more than one polymer into core-shell nanofibres. An example of such fibres, are fibres with a different polymer used for the core of the fibre than the shell. This technique was selected as a means by which coaxial nanofibers for this study were going to be fabricated. Nylon 6 was chosen as the core to be incorporated into SMI-P (as illustrated in **Figure 1.1**) because of its high mechanical integrity and insolubility in similar solvents to SMI-P. This allows for easier optimization of the coaxial electrospinning system. The dip coating technique was also evaluated in the fabrication of coaxial nanofiber mats. For this technique, electrospun nylon 6 nanofibres were dip coated with SMI-P and formation of the core shell structure was investigated.
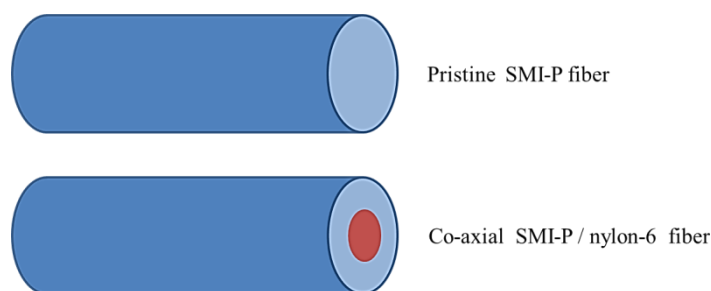
Figure 1.1: Visual representation of coaxial fibres

1.3   Problem statement

In water filtration, high pressures are present and biofilms (bacteria colonies) tend to grow on the filters. Thus, fibres that can withstand the high pressures in filtration systems as well as eliminating growth of bacteria are necessary. The polymer, SMI-P possesses

exceptional antimicrobial activity yet appalling mechanical properties, thus limiting its application in pressured filtration systems. This study will extend the excellent properties of the polymer by enhancing its mechanical properties allowing the polymer to be holistically applied in filtration unit.

1.4   Objectives

The main aim of this project was to strengthen SMI-P fibres to allow them to withstand high filtration pressures and to maintain the antimicrobial properties of the SMI-P fibres. To achieve these aims, the following objectives had to be met:

1. Synthesise SMI-P and fully characterize the polymer.
2. Coaxial electrospinning with nylon 6 as the core and SMI-P as the shell.
3. Coat nylon 6 mats with SMI-P as an alternative way to make the coaxial fibres.
4. Perform tensile tests to confirm that reinforcement of the fibres occurred.
5. Determine whether the SMI-P retains their antimicrobial.
6. Compare the antimicrobial activity together with the tensile strength of the coaxial mats (electrospun vs coated).

1.5   Thesis layout

Chapter 1: Is the introduction chapter that gives a brief overview of the relevance of nanofibre technology in water filtration. The chapter also states what problems may arise and how to overcome them. It also highlights the motivation for the study. The aims and objectives of the study are also outlined.

Chapter 2: Provides literature review giving an overall review of the main theory used in this study and explains the electrospinning process. The chapter also outlines the techniques used to fabricate coaxial nanofiber mats as well as details on the polymers used in this study are explained. The justification for the chosen techniques are also given.

Chapter 3: The experimental chapter reports on the experimental procedures that were used to achieve the objectives of this research project. These include details on the synthesis of the polymers and characterization techniques.

Chapter 4: The results and discussion chapter reports on the results of the characterization of the synthesized polymers as well as the fibres. The results of the mechanical tests and the antimicrobial tests are reported and compared to literature.

Chapter 5: This chapter provides the conclusions that were drawn from the findings of the study and recommendations for future work.

1.6   References

1.   Jain, P.; Pradeep, T., Potential of silver nanoparticle–coated polyurethane foam as an antibacterial water filter. *Biotechnol Bioeng* **2005,** *90*, 59-63.

2.   Ofra, A.; Yehuda, K., Bacterial growth in water. *Environmental Toxicology* **1989,** *4* (3), 363-375.

3.   Zodrow, K.; Brunet, L.; Mahendra, S.; Li, D.; Zhang, A.; Li, Q.; Alvarez, P. J. J., Polysulfone ultrafiltration membranes impregnated with silver nanoparticles show improved biofouling resistance and virus removal. *Water Research* **2009,** *43*, 715-723.

4.   Botes, M.; Cloete, T. E., The potential of nanofibers and nanobiocides in water purification. *Crit Rev Microbiol* **2010,** *36*, 68-81.

5.   Gule, N. P. Electrospun antimicrobial and antibiofouling nanofibres. Stellenbosch University, Stellenbosch, 2011. PhD

6.   Li, Q.; Mahendra, S.; Lyon, D. Y.; Brunet, L.; Liga, M. V.; Li, D.; Alvarez, P. J. J., Antimicrobial nanomaterials for water disinfection and microbial control: Potential applications and implications. *Water Research* **2008,** *42*, 4591-4602.

7.   Barhate, R. S.; Ramakrishna, S., Nanofibrous filtering media: Filtration problems and solutions from tiny materials. *Journal of Membrane Science* **2007,** *296*, 1-8.

8.   Bshena, O. E. S. Synthesis of permanent non-leaching antimicrobial polymer nanofibers. University of Stellenbosch, Stellenbosch, 2012. PhD

CHAPTER 2

Literature review

2.1   Polymer fibres

Synthetic polymer fibres are man-made fibres, which are usually made from synthetic polymers. The synthetic polymers are made from chemicals rather than natural materials such as cellulose and wood pulp.[1] These synthetic fibres have great potential in the medical and filtration industries since they can be chemically modified for different uses whereas natural fibres have limitations and cannot be chemically modified as much as synthetic polymer fibres. This gives rise to many more applications for synthetic polymer fibres as compared to natural fibres.[2] It is also easier to modify synthetic polymer fibres for unique end uses such as molecular alignment relaxation in polymer optical fibres for sensing applications.[3] There are other end uses such as repairing of injured connective tissues and hollow fibres as heat exchangers in building heat recovery applications.[4-5]

2.2   Synthesis of polymer fibres

The last few decades, an increased demand of polymeric nanofibres in various industries such as medical, protective clothing and filtration has made it necessary to develop techniques to produce polymer nanofibres. There are many techniques already developed, but some of the main techniques are melt blowing, force spinning and electrospinning.[6]

2.2.1 Melt blowing: is a one step process that can produce materials in the micrometre scale and smaller. This process works by extruding a molten polymer through the orifice of a die and the fibres that come out of the die are elongated by means air drag and then the fibres are collected on a suitable collector to form a web. The melt blowing setup can be seen in **Figure 2.1**. The problem with the melt blowing process is the fact that, the smaller the sizes fibres get, the more difficult it is to make the orifice in the die small enough for the production of the nanofibres.[7]
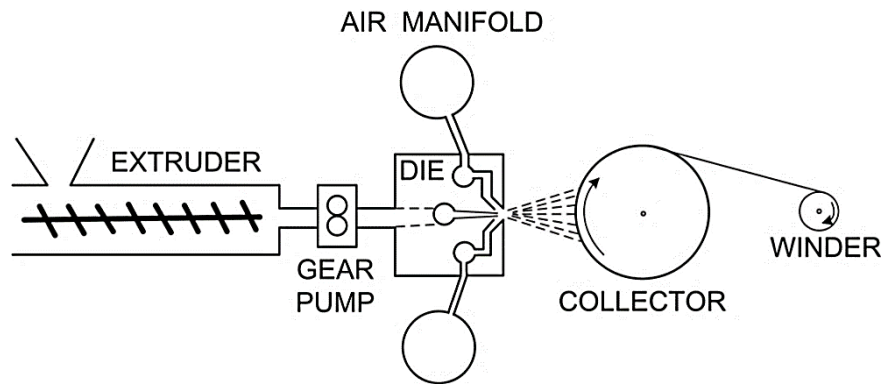
Figure 2.1: Melt blowing line schematic[8]

2.2.2 Force spinning: is a technique that uses a centrifugal force to spin nanofibres. The process involves a polymer solution that is placed in the spinneret and when the centrifugal force is high enough, the polymer is drawn out of the spinneret. As the polymer exits the spinneret, fibres are caught by the collector as shown in **Figure 2.2**. This process eliminates the high voltage needed by other techniques and the selection of spinnable materials are increased. This method is not that widely used and the equipment is not cheap.[9]
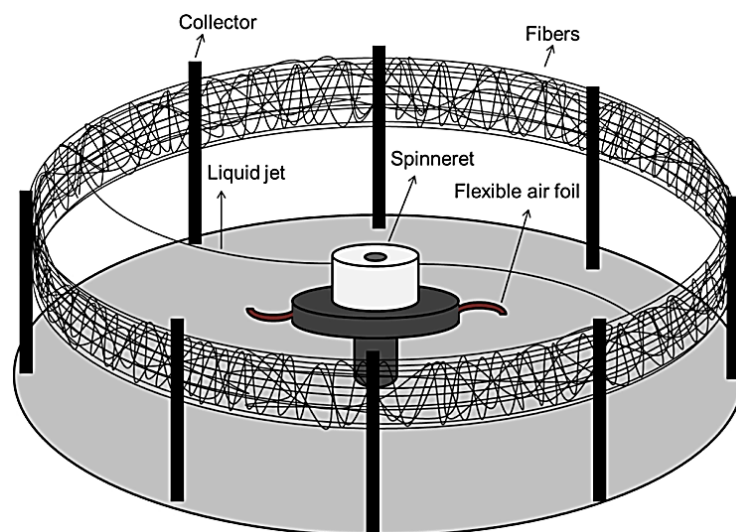
Figure 2.2: Force spinning schematic[10]

2.2.3 Electrospinning: is a widely used technique for producing nanofibers. It is an easy setup and produces uniform fibres with uniform sizes compared to the other techniques. The electrospinning technique can be modified to incorporate two different polymers and this is called coaxial electrospinning. The coaxial electrospinning setup produces a core-

19

shell fibre structure which are more difficult to produce by the other spinning techniques mentioned. For this study, the coaxial electrospinning technique was used to fabricate nanofibres with core-shell morphology.[6]

2.3   The electrospinning technique

Electrospinning has been around since the 1930s, but has attracted a lot of attention in recent years among researchers.[11] Its significance in the industrial market was however not readily available due to the low output, inconsistency, low molecular orientation and poor mechanical properties. In recent years, advances in the medical and filtration fields have reinitiated interest in the process. Until recent years, details on quantitative and scientific information about the process were very limited.[11] Electrospinning is a widely used technique for the production of polymer fibres in the micro to nanoscale.[12]

2.3.1   The process of electrospinning

The electrospinning process involves a syringe and needle (capillary) that is filled with a polymer solution. Then a high voltage range is applied to the needle to charge the polymer solution. The syringe pump that is used to supply a constant flow of polymer solution to spin constant fibres is activated and a droplet is formed at the tip of the needle. The syringe pump can be set to a variety of flow rates depending on what is needed by the specific polymer solution. The voltage applied induces a charge on the surface of the polymer droplet. Thus, the droplet becomes subjected to two opposing forces, which are the electrostatic repulsion force and the surface tension on the polymer solution. As the electric field increases the polymer solution at the tip of the needle elongates to make a cone and this is known as the Taylor cone. As the electric field is increased, the critical point of where the repulsion force overcomes the surface tension is reached and so a charged jet of polymer solution is then ejected from the tip of the Taylor cone. The jet moves away from the tip and enters a region of instability. Then the jet undergoes a whipping process because of the electrostatic repulsion force from the same charged ions in the electrospinning jet before it gets to the collector as a dried nanofibre. The whipping that takes place allows for stretching of the charged jet and so decreases the fibre diameter from micro to nano scale while the solvent evaporates off. This results in the dry fibres landing on the collector plate to make a nonwoven mat of nanofibres.[13] **Figure 2.3** shows the setup of the electrospinning system as described.
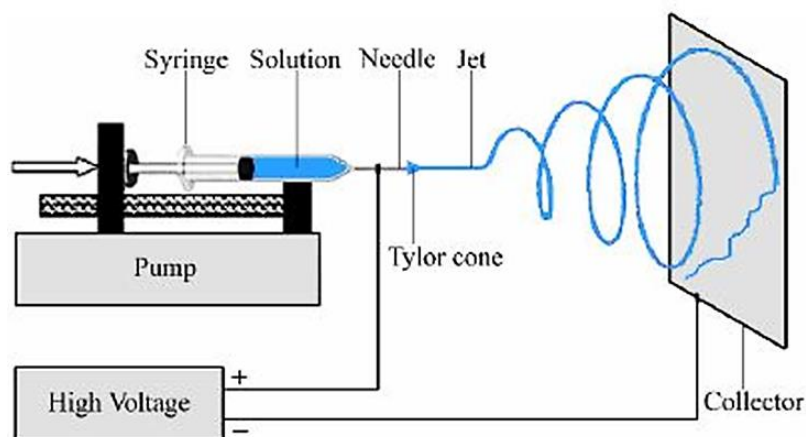
Figure 2.3: Single needle electrospinning setup[14]

2.4   Applications of electrospun nanofibres

The applications of electrospun fibres have grown vastly over the years and these fibres are now used in different areas.[15] Figure 2.4 summarizes the applications of nanofibre membranes. Electrospun fibres also used in water filtration, biotechnology and sensors, and investigations are underway to find more applications for these fibres where fibre alignment is not a requirement.[16] Research has shown that ordered structures can outperform disordered structures hence the vast number of studies to produce more ordered structures rather than disordered ones.[16] Current research on electrospun fibres and industrial applications are restricted to non-woven, but this technology is heading towards more elaborate structures.[16] The fact that the electrospinning process does not work on all kinds of polymers brought forth the realization that some polymers are unspinnable. This propelled research in the field towards realizing means in which such polymers can be electrospun as well. This gave rise to the advancement in electrospinning and hence the development of coaxial electrospinning.[17]
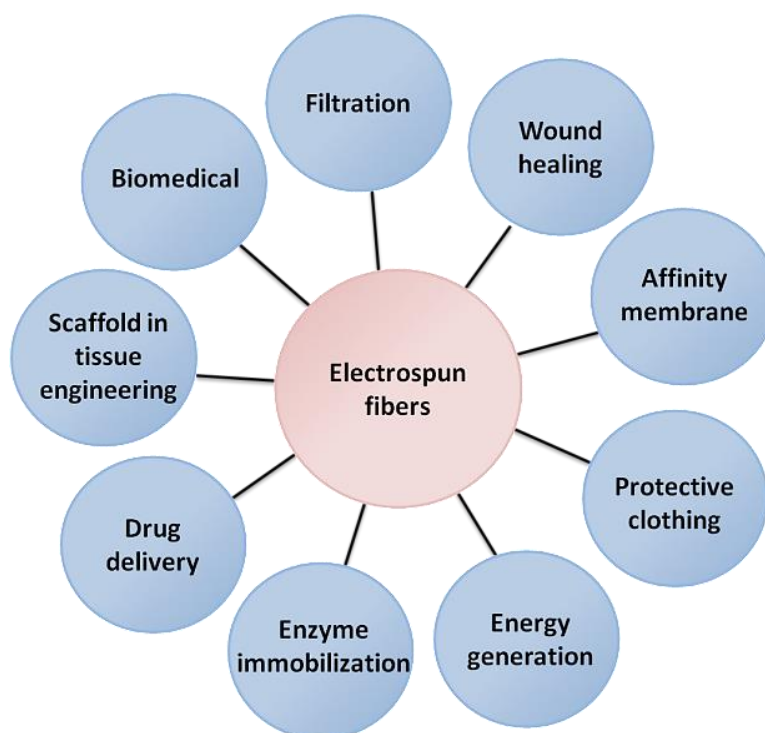
Figure 2.4: Diagram of the possible applications of electrospun nanofibres[18]

2.5   Coaxial electrospinning

The electrospinning technique can be modified to give fibres with different morphologies. Altering the type of needles used as well as the type of solutions that are used would affect the morphology.[19] This opened the door to make composite fibres that can function as drug delivery systems or even make self-healing polymers.[20-21] These advances in electrospinning gave rise to techniques like melt electrospinning, emulsion electrospinning and also coaxial electrospinning. The melt electrospinning technique is a process whereby the production of fibrous structures is made from polymer melts and avoids the requirement to make polymer solutions first which eliminates the limitation of solvents that can be used.[22] Melt electrospinning has been used in the tissue engineering, textiles and filtration fields.[23] The emulsion technique can be used to produce core-shell fibres as it uses a water in oil emulsion. This works by having the potential core in water and the polymer to be used for the shell is dissolved in the oil (organic) solvent that needs to evaporate faster than water. These two solutions are mixed together to form the emulsion and placed in the single needle syringe to electrospin the fibres. The emulsion electrospinning process produces core-shell fibres by the fact that the organic solvent has a low boiling point, the emulsion partially de-emulsifies and the viscosity of the oil phase

increases much faster than that of the water phase. Thus, the viscosity gradient that is formed causes the water layer to move to the inner space which leads to the core-shell structure. Thus, the emulsion technique does not require a modified needle as coaxial requires, but the fibres are harder to produce than the ones made by the coaxial technique since extra parameters are need (one polymer must be able to move to the core of the other) to produce the core-shell fibres. Thus, due to the fact that emulsion electrospinning does not work for all combinations of polymers it is easier to perform coaxial electrospinning as it works for more combinations than emulsion electrospinning.[24]
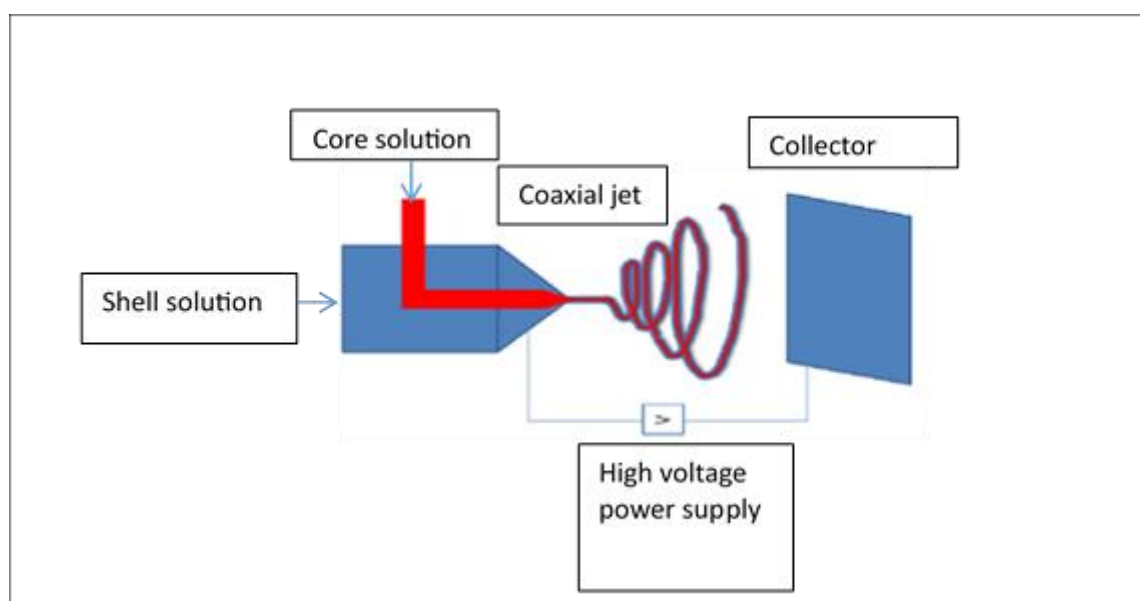
Figure 2.5: The electrospinning setup for a coaxial system

Coaxial electrospinning is a modification of the electrospinning technique to allow for the incorporation of different polymer solutions into one fibre. The technique uses multiple solution feeds in the injection process and so one solution can be injected into the core of another solution to produce core-shell fibres. The setup of the coaxial system can be seen in Figure 2.5. The shell of the fibre is thought to act as a carrier for the core solution at the Taylor cone of the electrospinning jet. The solutions that are used should be immiscible in order to observe the core-shell structure. This results in the fibres with distinct phases because of phase separation during the solidification of the nanofibres, but it is also possible to produce the core-shell structure with miscible polymer solutions except that it is harder to optimise the electrospinning process.[19]

The coaxial electrospinning technique provides a new range of applications due to the unique fibres that are produced and their unique mechanical properties. These core-shell fibres can be used in various fields since they have unique properties and characteristics.[25] These fibres tend to have higher break energies than single polymer fibres and so can be used in previously unusable areas. The core-shell fibres can be used in different fields such as in lithium ion batteries, solar cells, luminescence, super capacitors, environmental remediation, filtration and more.[25]

2.6   Parameters

The electrospinning technique is complex and many of the parameters and processes are dependent on one another. Thus, changing one parameter may affect another, for example, increasing the dielectric constant of a solution by replacing the solvent can affect the surface tension, conductivity and in the end, polymer chain entanglement. This fact makes it difficult to get the ideal conditions for electrospinning and because of these intertwined effects. There is no general set of processes, system parameters and ambient parameters that can be used to ensure continuous electrospun fibres that are uniform for a given polymer solution.

In the case of coaxial electrospinning, controlling these parameters becomes very important because to have continuous core-shell fibres the stability between the parameters must be obtained. The factors that can affect the stability of the electrospinning process are discussed in literature.[26-27] If ideal conditions for coaxial electrospinning are to be met, both solutions must be sufficiently viscous as well as spinnable (at the very least, the shell should be spinnable). The polymer solutions should be immiscible, but they can also be miscible although this makes the optimization of the electrospinning harder.[27] **Section 2.6** discusses the most significant process parameters for coaxial electrospinning.

2.6.1   System parameters

1.6.1.1 Miscibility of core and shell solutions

Research done by Li and Xia reported that the most critical parameter in the continuous and uniform formation of fibres that can also be used for making hollow fibres is the immiscibility of the core and shell solutions.[28]

While Sun *et al*. showed that for well-defined core-shell fibres mixing of two polymer solutions must be avoided. This can be achieved by electrospinning the core-shell as a high rate. Such is possible due to the fact that polymers have lower diffusion coefficients compared to the rate at which fibres stretch/solidify.[29-30] The miscible core-shell solutions used for the electrospinning solutions produce poorly defined interfaces as to the better-defined interfaces from the immiscible core-shell solvents. Other researchers have also shown that using the same solvents will reduce the interfacial tension produced between the two solutions. This may aid viscous drag (is the frictional forces that causes a fluid to move backwards and the obstacle forward) by the shell solution on the core and also may produce more effective core entrainment. Thus the core is spread everywhere in the core-shell fibres.[31] Thus the viscous drag allows for the core to be moved forward with the shell instead of the shell only being electrospun.

2.6.1.2 Effect of solution concentration, viscosity and molecular weight

Coaxial electrospinning can only occur if the shell solution was spinnable before by means of single needle electrospinning and readily formed continuous fibres. Thus the shell polymer needs to have significant polymer chain entanglement in solution ($\geq$ 2.5 entanglements per chain).[32] The number of entanglement in solution is determined by the molecular weight and concentration of the polymer and in turn determines if stable fibres are formed. If the shell solution contains less than 2.5 entanglements per chain it would result in instable electrospinning and so produces a beading fibre morphology or possibly electrospraying of droplets. The use of a shell solution with < 2.5 entanglements per chain would result in insufficient wrapping of the core polymer. If the core concentration is too low it would result in a discontinuous core in the fibres and the jet breaks up.[26, 33]

The diameter of coaxial fibres obtains a broad distribution by increasing the core concentration, but this has no effect on the morphology of the fibres.[34] It was also reported that with an increase in core concentration, the total fibre diameter increased with the shell becoming thinner.[35] If the parameters for electrospinning are kept constant and the shell solution concentration is increased the larger the shell thickness will become although the core will be smaller. The inverse would happen with a lower shell solution concentration.[36-37]

2.6.1.3 Solvent volatility

The volatility of the solvents used during electrospinning influences the time available for the stretching of the jet as well as the alignment of the polymer molecules. If the solvents are highly volatile they will evaporate too fast, which will prevent the optimal viscosity from being achieved. Thus the alignment of the polymer molecules as well as the stretching of the jets to form thin, smooth and uniform fibres is inhibited.[27]

If the solvent volatility is too high the Taylor cone can form a skin on its surface which will eventually block the needle and stop the electrospinning. Then for electrospinning to continue the blockage would have to be removed for the renewal of the droplet. [38]

If the solvent volatility is too low, it would cause a low evaporation of the solvent and so it can remain in the fibres. This causes wet-fused fibres can be collected. Thus, toxic residues from the slow evaporation of the solvent may restrict applications.[39]

Solvent volatility plays a big role in the formation of the nanostructures by influencing the phase separation process, which occurs when the fibre solidifies and dries. Thus the higher the solvent volatility is, the higher the rate of phase separation, which makes more porous structures in relation to low solvent volatility.[39]

The effect of solvent volatility can be influenced by the ambient conditions like the relative humidity, which is discussed in **Section 2.6.3**. Solvent mixtures are used to increase or decrease the volatility of the solutions in order to produce stable spinning as well as changing the kinetics of the phase separation to produce certain fibre morphologies.[40]

2.6.1.4 Conductivity

The electric field that is formed from the charge applied, forces the ions in the polymer solution to move in this field and so the force generated from this is transferred to the polymer solution. The higher the conductivity of the polymer solution, the more readily the electrospinning process occurs and so a greater force is applied to the ions.[41] The opposite also occurs where non-conductive polymer solutions will not spin easily without some assistance.[42] The use of either a conductive shell or core solution can allow that solution to pull a respective non-conductive core or shell solution which allows for the non-conductive solution to be electrospun.[43] The charge density of the electrospinning fluid jet is determined by the electrical conductivity of a polymer

solution. Under a constant electrical field the higher the conductivity of a polymer solution is the greater the electrical force is that the jet experiences and so the stretching of the jet is greater along its axis and so the fibre diameter of the fibres produced would be smaller.[43]

Rayleigh instability is opposed to the surface charge density and the whipping and bending instabilities of the jet and acts to enhance the whipping and bending of the jet. The production of fine fibre diameters is very dependent on the conductivity of the solutions in the cause of dilute solutions, where beading can be a problem. The use of polar solvents or the addition of salts to polymer solutions can lead to reduced bead formation during the electrospinning process.[43-44]

A core solution that has a higher charge density than that of the shell solution causes the electric field produced during coaxial electrospinning to pull the core at a higher rate that is supplied by the syringe pump. Thus, causing a discontinuous flow of the core solution forming a core-shell structure that has missing core polymer at certain points.[30]

The coaxial electrospinning system that has a shell with higher solution conductivity causes the greater elongation of the whipping of the jet and so forms thinner fibres that have thinner cores.[30]

2.6.1.5 Dielectric constant

The dielectric constant is a solution's ability to hold a charge as well as dispersion of the charge and the extent at which a material can concentrate electric flux. It is also related to the charge density of a solution. Thus, the higher the dielectric constant the more evenly the surface charge density is dispersed, which improves the uniformity of the fibres. Then also the higher the dielectric constant, the finer the fibre diameter becomes.[45]

2.6.1.6 Surface tension and interfacial tension

The initiation of a jet is determined by a range of important parameters and one of these parameters is surface tension. Since there is a critical amount of charge that is needed to overcome the surface tension in the Taylor cone and in order to eject a jet of the polymer solution from the apex.[46]

The nature of perturbations experienced by the whipping jet is determined by the balance between the columbic repulsions and the surface tension in the electrospinning jet. The

surface tension of the polymer solution causes Rayleigh instability, but it can be countered by the viscosity of the solution (entanglements) as well as the electrical Maxwell forces. The formation of beads tends to occur when a solution has a high surface tension.[47]

The polymer concentration variation has less of an effect on electrospinning since the surface tension is mainly a function of the solvent. The addition of salts and surfactants can be used to reduce the surface tension.[43]

The stability of the Taylor cone as well as the translation of the shear forces from the shell solution to the core is affected by the interfacial tension between the core and shell solutions. Low interfacial tension of the core and shell solutions are wanted (miscible or almost miscible solvents) since they allow for the viscous dragging forces of the shell solution to drag the core continuously and form uniform core-shell fibres.[26]

2.6.2   Process conditions

2.6.2.1 Electric field strength applied voltage, spinning/gap distance

The electrical field strength, applied voltage and spinning distance are related parameters. A simplified form of the electric field strength is described as the applied voltage over the spinning distance and is expressed as kV/cm. If the voltage on a core-shell droplet is increased it will affect the droplet as depicted by **Figure 2.6**. The surface charge on the jet is caused by the applied voltage. Thus, the higher the applied voltage the higher the instability of the whipping jet becomes. This is important in coaxial electrospinning to have stretching of the shell solution, which will in turn pull the core solution with to form core-shell fibres. If the voltage goes above a certain threshold, the Taylor cone of the core-shell system will be forced to split into two jets in order to distribute the charge on the surface of the Taylor cone.[43, 46,48]
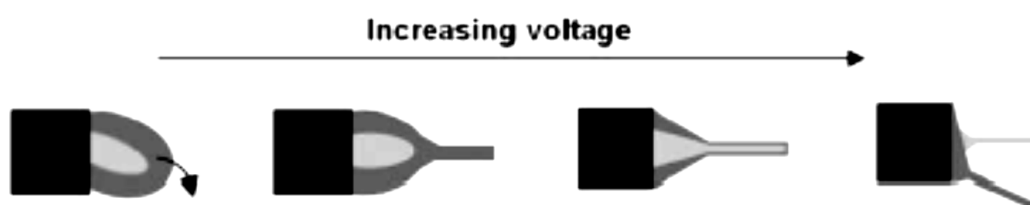
Figure 2.6: The effect of increasing applied voltage on the core-shell droplet[48]

An increase in the electric field strength can generally be used to reduce the core-shell fibre diameters.[28] In the event that the solution feed rates are increased at the same time as the electric field strength, the reduction of fibre diameter mentioned before will not occur. Higher volumetric flow rates are caused by the increase of electrostatic forces and so more solution gets pulled out of the spinneret. Solutions with high viscosities possess a higher surface tension and require a larger build-up of electric charge as well as a larger electric field strength to electrospin.

The capillary and collector geometry as well as the electric field strength (potential difference/distance) determines the nature of the electric field lines of a elecrospinning gap between the needle and the collector. The electric field lines are the unseen force produced by the electric charge that produces an electric field to pull the fibres towards the collector.[49]

The pulling forces on the fluid jet are enhanced by a larger electric field for the same surface charge density and this also increases jet thinning and molecular orientation.[47]

The distance between the capillary opening and the collector plate is known as the spinning distance. The spinning distance has an influence on different aspects of electrospinning such as the electric field strength, it also determines the time available for whipping to occur and it also determines the time for solvent evaporation before the fibres hit the collector plate. The increase of the spinning distance along with the adjustment of the other parameters would reduce the fibre diameter due to more time for the whipping instability as well as for solvent evaporation. If the spinning distance is decreased, it can cause wet fibres to form, which in turn can form a network of connected fibres due to solvent diffusion where the fibres overlap. In the case where the distance between the capillary and the collector is too small it can cause corona discharge to occur.[31]

2.6.2.2 Applied voltage polarity

The mobility of the charges in polymer solutions is reported to be significantly affected by the polarity of the applied voltage. The fibre diameters produced by a negatively charged solution are shown to be larger and the negative charge also causes the electrospun area on the collector to become smaller. The use of AC voltages allows for greater alignment of fibres to occur.[50-51]

2.6.2.3 Flow rate

The rate at which the core and shell solutions are fed to the spinneret should be able to maintain a continuous core-shell jet as well as have optimum stability for the core entrainment. The use of a flow rate for the core solution that is too high for sufficient solvent evaporation to occur will cause the core jet to break up into droplets within the fibre. In the case where the shell solution has a flow rate that is much higher than the core solution flow rate it will cause a non-continuous core structure within the shell structure.[30,34] Thus, for coaxial electrospinning it is easier to optimise the system using flow rates that are close together for the core and shell solution.

The core and shell component's ratios can be manipulated by using the core-shell flow rates. As such by increasing the flow rate of the core it will result in a larger core diameter and a thinner shell diameter.[35] The use of a core flow rate that is past a certain threshold on low molecular weight cores will cause the fibres to collapse due to the shell wall having become too thin to support the core. The increase of the shell flow rate causes the shell wall thickness to increase and will in turn decrease the relative volume of the core.[37]

2.6.2.4 Capillary tip

The effective charging of the electrospinning solution requires a narrow electrode. It has been said that a smaller diameter capillary would produce smaller fibres in single capillary electrospinning, but the effects of the capillary size on the core-shell fibres diameter that is spun by the coaxial electrospinning setup has not yet been specifically reported on.[52]

2.6.2.5 Core-needle protrusion

The attempt to produce core-shell fibres from the entrainment of a core solution does not always work as described in the paper by Reznik *et al.*[53] The rapid movement of free charges from both solutions as well as their interface to the free surface of the shell solution can be the cause for failure to produce core-shell fibres. This makes the electric field only act on the free surface. This problem can be overcome by the extension of the core capillary by a distance that is half the radius of the shell capillary. Thus, causing the core solution to be brought closer to the free charge surface where the best charge density and viscous drag is felt. The entrainment and concentricity problems can be corrected by

using the single nozzle which removes the need for a core capillary and this core-shell electrospinning technique was proposed by Bazilevsky *et al*.[54] The single nozzle has a solution that contains both the core and shell polymer and then it relies on the core solution droplets to precipitate. The precipitate becomes trapped at the base of the Taylor cone issuing the shell solution jet from its tip. The shell solution's flow needs to be strong enough to stretch the core droplets into the Taylor cone which should form the core-shell jet. This method will however not apply to all core-shell solution combinations.[19]

2.6.2.6 Coaxial spinneret configurations

The capillary in capillary configuration is the most common coaxial electrospinning needle setup and is discussed in Section 2.5.[26] There is also the L-shaped configuration (Figure 2.7), which is a simpler design and has been used successfully. The L-shaped configuration does not require a specialized needle as required by the capillary in capillary configuration. The L-shaped method uses two individual single needles of which the one used for the shell solution is larger than the one used for the core solution and so the small needle is inserted into the Tylor cone of the larger needle whereby producing a coaxial Taylor cone. The positive charge applied for electrospinning is only placed on the large needle and not the smaller needle as the shell solution drags the core solution when it is electrospun. The capillary in capillary method is the one used in this study as it is a more widely used technique than the L-shaped method. The L-shaped method is described in more detail by Wang *et al*.[37]
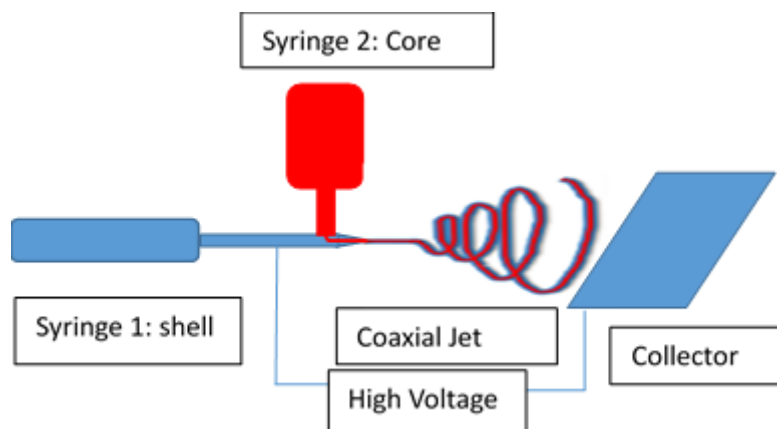
Figure 2.7: L-shaped coaxial electrospinning set-up

2.6.2.7 Collector

Conductive receptors can be used for fibre collection or the fibres can be intercepted on its way to such collectors. The conductive receptors can be dynamic or static and may be grounded or positively charged. There are a variety of collectors that can be used to collect the non-woven or aligned fibre mats. It is also possible to spin directly onto a substrate.[31,55] The use of either an electrostatic gap alignment collector or water bath method can be used to make yarns shown by Smit *et al*.[55] The method of spinning onto a water bath may influence the fibre morphology and allows the toxic non-volatile solvents to be removed. The numerous collectors to collect electrospun fibres are described in detail by Theo and Ramakrishna.[49]

Regarding the packing densities of the fibres, the dielectric properties of the materials used as collectors are of importance. The fact that polymer fibres are generally good insulators will dilute the conducting effect due to the fibres piling onto each other after the initial fibres cover the collector and so the repulsion occurring between the successive fibre layers increases. The gap alignment collector shown in Figure 2.8 does not have space for the fibres to get pushed into space because of the charged fibre repulsion once the first layer of fibres is deposited. Thus, there is no parallel alignment of the fibres between the gaps and so less ordered than the first gap aligned fibres. This allows the fibre mats to have a lower packing density and so creating a more open structure. The use of a rotating collector can improve the alignment of the fibres by using a higher linear collecting velocity.[31]
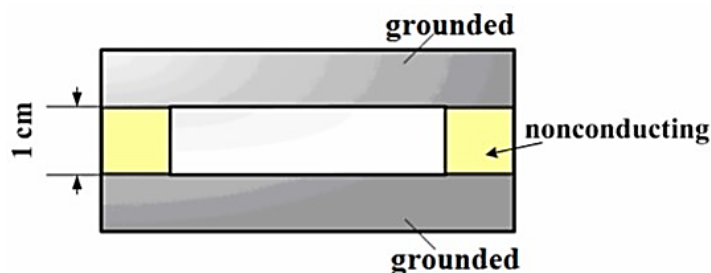
Figure 2.8: Gap alignment collector[56]

2.6.3 Ambient conditions

It is standard for most electrospinning experiments to be done under normal atmospheric conditions. The polymer and the solvent as well as the ambient conditions used for the electrospinning process can be used to control the surface area, surface morphology and more specifically the surface porosity (size, shape, density and depth of pores).[38, 57]

The surface area needs to be controlled by the formation of pores on the individual fibre surfaces since it is important for some applications such as drug release media or filtration applications. The deposition of nanoparticles onto the fibre surface (and inside the pores) requires porous surface features of a known size and distribution. The incorporation of drug molecules in the core of core-shell fibres for the controlled release of the drug through the fibre pores also requires the porous surface features of a known size and distribution.[38,57]

Electrospinning in humid ambient conditions with solvents that have high vapour pressures produce fibres with porous/rough surfaces. In an atmosphere with a relative humidity above 30% it has been shown that surface features and/or pores occur.[57] The shape distribution, diameter and the number of the pores increase when the humidity is raised. The use of polymers with higher molecular weights will result in bigger non-uniformly shaped pores.[57]

Vapour-induced (VIPS) and thermally-induced (TIPS) phase separation are the two mechanisms of phase separation that are attributed to the porosity seen in electrospun fibres.[38] TIPS is caused by the lowering of the temperature on the fibres due to solvent evaporation and VIPS is caused by the absorption of water vapour taken from the atmosphere. The surface feature called breath figure is another type of surface feature that is due to similar mechanisms.[41] The rapid solvent evaporation causes the evaporative cooling of the electrospinning jet surface. Electrospinning at different relative humidities can cause the observation of different morphologies.[38, 58-59]

Controlling the electrospinning environment helps to control the solidification rate of the spinning jet because by controlling the evaporation it allows for the sufficient jet elongation to produce fine fibres. This can be done by electrospinning in various atmospheres, controlling the humidity and temperature of the electrospinning environment. The use of the gas-jacketed capillary tip to spin with would be another method of controlling the electrospinning environment around the spinneret and the jet.

This would allow the jet to get surrounded with gas that is saturated with solvent to stop drying and promote a stable Taylor cone at higher voltages.[40] The use of a gas jacket that has high air pressure may induce more drag which allows for enhanced drawing of the fibre and this process is called electroblowing. The use of a heated air jacket or heating lamp is another way to influence the drying rate.[60]

2.7   Choice of polymers

Nylon: Nylon also known as polyamide is a synthetic material and has many advantages such as having resistance to heat. Nylon 6 is a semi crystalline polyamide, but unlike most other nylons it is synthesised by means of ring opening polymerization as shown in Figure 2.9. Nylon 6 is used for different applications such as for clothing, used to make gears, fittings, bearings and a lot more. For all these applications, nylon 6 is presented as a strong material. It was for its inherent properties that nylon 6 was chosen in this study to improve the strength of otherwise brittle fibres.[61] These inherent properties are the toughness of the nylon fibres, high tensile strength and elasticity. The amide group in nylon allows hydrogen bonding among the polyamide chains and that is what gives nylon such a high strength at elevated temperatures, as well as its toughness at low temperatures. It is highly abrasion resistant and also chemically resistant to chemicals such as acids and alkalis.[59] Thus the fact that we are looking for a polymer that possesses high tensile strength to reinforce the SMI-P and not affect the antimicrobial properties, nylon 6 is a good polymer for the reinforcement of SMI-P since it has great tensile strength as shown by all its applications.
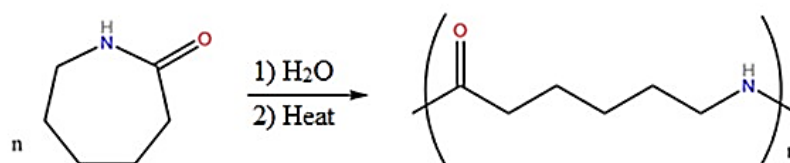
Figure 2.9: Reaction scheme for the synthesis of nylon 6 via ring-opening polymerization[61]

Poly(styrene-co-N-(N',N'-dimethyl-3-aminopropyl)maleimide) (SMI-P): SMI-P is a polymer that is synthesised by the modification of poly(styrene-*co*-maleic anhydride) with *N,N*-dimethyl-3-aminopropyl-1-amine as shown in Figures 2.10 and 2.11. [31, 62]
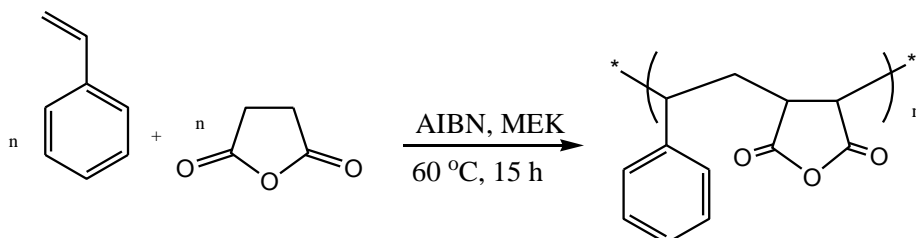
Figure 2.10: Radical alternating copolymerization of styrene and maleic anhydride[62]
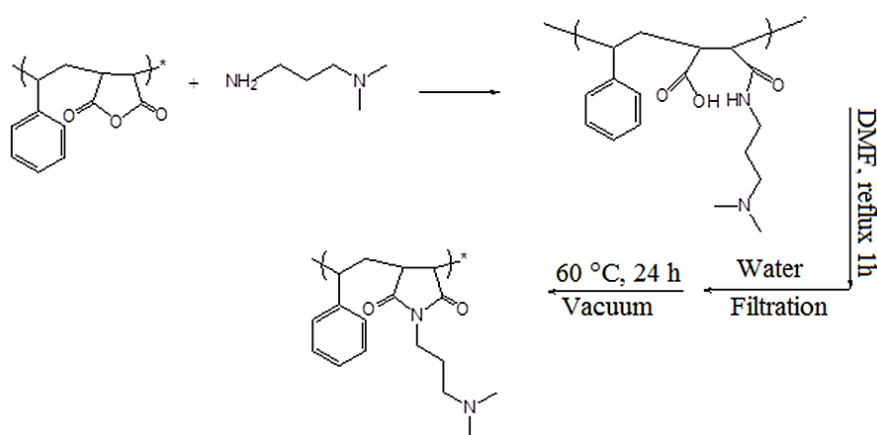
Figure 2.11: Imidization and ring closure of the SMA to SMI-P[62]

2.8   Coatings

Coatings are applied to the surface of an object, which is called a substrate and these coatings are coverings that can be functional, decorative or both. These coatings do not need to cover all the substrate and can be used for localized use. These localized coatings can be seen on the labels of soft drink bottles as only a specific region has an adhesive part to keep the label on the bottle. Then paints are coatings that mostly represent the functional (as a protection cover) and decorative properties. The functional coatings can be used to change the surface properties such as for adhesion, wettability, corrosion resistance or wear resistance and the coatings provide completely new properties to the substrate.[63-64]

Coatings have been used for a wide range of products such as wiring assemblies to protect them from moisture, handling, ionic contaminates and particulates. These coatings (polyurethanes, acrylics, epoxies and silicones) have been used for over 40 years.[65-66]

The basic requirements that a coating must meet depend on the specific application as well as the function that the coating needs to perform in the specific application. However there is one requirement which is basic to all functions and that is good adhesion during the operation of the substrate and during the lifespan of the substrate.[65,67]

There are many different functions for coatings such as changing the adhesive properties (make non-stick PTFE coated pans), optical coatings (anti-reflective coatings), catalytic (self-cleaning glass), and protective (anti-corrosion, antimicrobial).[65,67]

There are many ways in which coatings can be applied. This study will focus on two techniques that are of particular interest for the coating of fibres, i.e. spin coating (Section 2.8.1) and dip coating (Section 2.8.2).

2.8.1   Spin coating

Spin coating is a process that is used to deposit a uniform thin film on a flat substrate. This is done by dropping a small amount of the coating material in the centre of the substrate while a low spinning speed is applied and then the substrate is spun at a high speed to spread the coating material by means of centrifugal force. The coating thickness can be altered by adding more of the coating material during the rotation and the longer the spin coater spins the more fluid spins off the edges and a thinner coating is applied. Figure 2.12 represents a spin coater.[68]
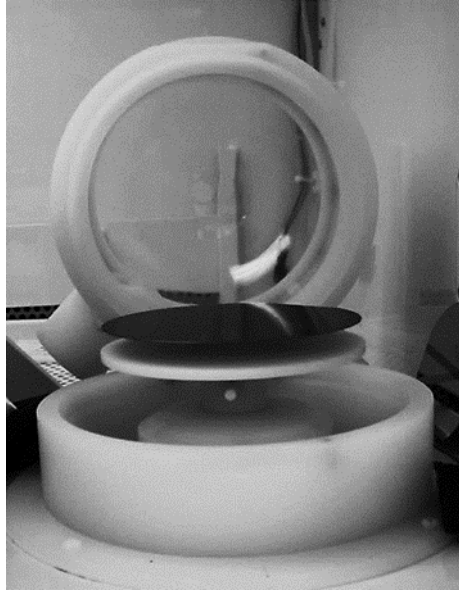
Figure 2.11: Spin coater equipment[68]

2.8.2   Dip coating

Dip coating is an industrial process whereby substrates such as fabrics are coated. For more flexible substrates, the process is made into a continuous process where the substrate is dipped into the coating solution and then is run out over rollers to remove excess fluid after which the substrate with the coating can dry. Figures 2.13 and 2.14 represent types of dip coating.[68-69]
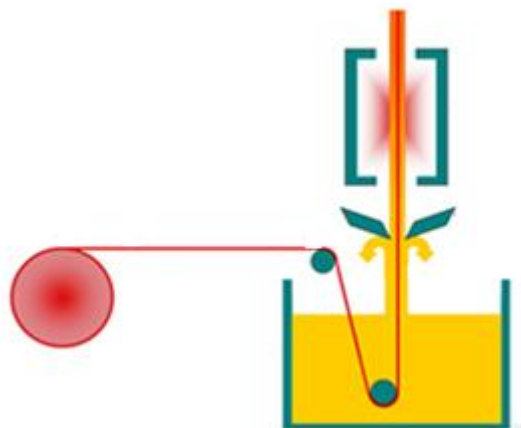
Figure 2.12: Process for continuous dip coating[64]
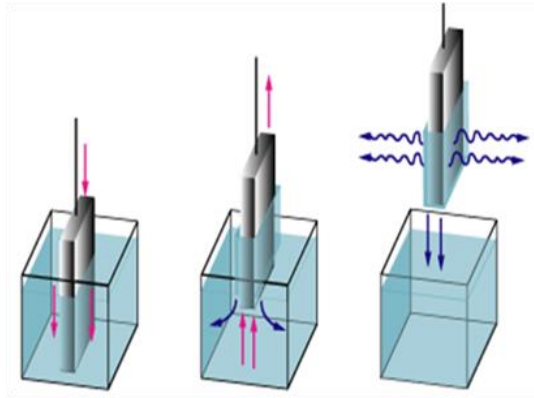
Figure 2.13: Experimental setup for batch-wise dip coating[64]

For this study, dip coating nylon fibres in solutions of SMI-P was evaluated. The aim was to fabricate strong nanofibres with a nylon-6 core and a SMI-P shell, thus retaining the antimicrobial properties of the shell polymer.

2.9   Reinforcement methods for SMI-P

This study's aim is to reinforce SMI-P fibres without negatively affecting the antimicrobial activity. Thus, two methods were decided on to reinforce SMI-P. The methods used were capillary in capillary coaxial electrospinning and dip coating. The capillary in capillary system was decided on because it is a more widely used method than the L-shaped coaxial method as described in Section 2.6.1 and the capillary in capillary method needle setup was already available for this study. The coating process was decided on because it is an easy alternative to the coaxial method. The dip coating method was decided on over the spin coating method because it is a cheaper method. It is more suited for mass production than spin coating. This is required for the water filtration end use and so dip coating was performed for this study.

2.10   References

1.   Preston, J. Synthetic fibre. https://global.britannica.com/technology/synthetic-fiber.

2.   Karen, S. Advantages & disadvantages of natural fibers. http://www.ehow.com/list_6887650_advantages-disadvantages-natural-fibers.html.

3.   Stajanca, P.; Cetinkaya, O.; Schukar, M.; Mergo, P.; Webb, D. J.; Krebber, K., Molecular alignment relaxation in polymer optical fibers for sensing applications. *Optical Fiber Technology* **2016,** *28*, 11-17.

4.   Lee, N. M.; Erisken, C.; Iskratsch, T.; Sheetz, M.; Levine, W. N.; Lu, H. H., Polymer fiber-based models of connective tissue repair and healing. *Biomaterials* **2017,** *112*, 303-312.

5.   Chen, X.; Su, Y.; Aydin, D.; Reay, D.; Law, R.; Riffat, S., Experimental investigations of polymer hollow fibre heat exchangers for building heat recovery application. *Energy and Buildings* **2016,** *125*, 99-108.

6.   Nayak, R.; Padhye, R.; Kyratzis, I. L.; Truong, Y. B.; Arnold, L., Recent advances in nanofibre fabrication techniques. *Textile Research Journal* **2011,** *82*, 129-147.

7.   McCulloch, J., The history of the development of meltblowing technology. *Int Nonwoven* **1999,** *8*, 139-149.

8.   Hiremath, N.; Bhat, G., Melt blown polymeric nanofibers for medical applications. *Nanoscience & Technology* **2015,** *2*, 1-9.

9.   Weitz, R.; Harnau, L.; Rauschenbach, S.; Burghard, M.; Kern, K., Polymer nanofibers via nozzle-free centrifugal spinning. Nano Letters **2008,** *8*, 1187-1191.

10.   Yanilmaz, M.; Zhang, X., Polymethylmethacrylate/Polyacrylonitrile membranes via centrifugal spinning as separator in li-Ion batteries. *Polymers* **2015,** *7*, 629-643.

11.   Young, D. S. Hyaluronic acid-based nanofibers via electrospinning North Carolina State University, North Carolina, 2006.

12.   Li, D.; Xia, Y. N., Electrospinning of nanofibers: Reinventing the wheel? *Advanced Materials* **2004,** *16*, 1151-1170.

13.   Cronje, L. Surface modification of styrene maleic anhydride nanofibers for efficient capture of Mycobacterium tuberculosis. Stellenbosch University, Stellenbosch, 2012. PhD

14. Ziabari, M.; Mottaghitalab, V.; Haghi, A. K., Application of direct tracking method for measuring electrospun nanofiber diameter. *Brazilian Journal of Chemical Engineering* **2009,** *26*, 53-62.

15. Lee, S.; Obendorf, S. K., Use of electrospun nanofiber web for protective textile materials as barriers to liquid penetration. *Textile Research Journal* **2007,** *77*, 696-702.

16. Teo, W.-E.; Inai, R.; Ramakrishna, S., Technological advances in electrospinning of nanofibers. *Science and Technology of Advanced Materials* **2011,** *12*, 1-5.

17. Guozhong CAO, C. J. B., *Annual review of nano research*. World Scientific Publishing: Singapore, 2006; Vol. 1, p 628.

18. Weistron Electrospinning technique. http://www.weistron.com/tech-abc/electrospinning-tech/.

19. Bazilevsky, A. V.; Yarin, A. L.; Megaridis, C. M., Co-electrospinning of core−shell fibers using a single-nozzle technique. *Langmuir* **2007,** *23*, 2311-2314.

20. Zeng, J.; Xu, X.; Chen, X.; Liang, Q.; Bian, X.; Yang, L.; Jing, X., Biodegradable electrospun fibers for drug delivery. *Journal of Controlled Release* **2003,** *92*, 227-231.

21. Sinha-Ra, S.; Pelot, D. D.; Zhou, Z. P.; Rahman, A.; Wub, X.-F.; Yarin, A. L., Encapsulation of self-healing materials by coelectrospinning, emulsion electrospinning, solution blowing and intercalation. *Journal of Materials Chemistry A* **2012,** *22*, 9138-9146.

22. Kristóf, Z.; Balogh, A.; Drávavölgyi, G.; Ferguson, J.; Pataki, H.; Vajna, B.; Marosi, G., Solvent-free melt electrospinning for preparation of fast dissolving drug delivery system and comparison with solvent-based electrospun and melt extruded systems. *Journal of Pharmaceutical Sciences* **2013,** *102*, 508-517.

23. Dalton, P. D.; Grafahrend, D.; Klinkhammer, K.; Klee, D.; Möller, M., Electrospinning of polymer melts: Phenomenological observations. *Polymer* **2007,** *48*, 6823-6833.

24. Xu, X.; Zhuang, X.; Chen, X.; Wang, X.; Yang, L.; Jing, X., Preparation of core-sheath composite nanofibers by emulsion electrospinning. *Macromolecular* **2006,** *27*, 1637-1642.

25. Qu, H.; Wei, S.; Guo, Z., Coaxial electrospun nanostructures and their applications. *Journal of Materials Chemistry A* **2013,** *1*, 11513-11528.

26.   Moghe, A. K.; Gupta, B. S., Coaxial electrospinning for nanofiber structures: Preparation and applications. *Polymer Reviews* **2008,** *48*, 353-377.

27.   Dror, Y.; Salalha, W.; Avrahami, R.; Zussman, E.; Yarin, A. L.; Dersch, R.; Greiner, A.; Wendorff, J. H., One-step production of polymeric microtubes by co-electrospinning. *Small* **2007,** *3*, 1064-1073.

28.   Li, D.; Xia, Y., Direct fabrication of composite and ceramic hollow nanofibers by electrospinning. Nano letters 2**004,** *4*, 933-938.

29.   Sun, Z.; Zussman, E.; Yarin, A. L.; Wendorff, J. H.; Greiner, A., Compound core-shell polymer nanofibers by co-electrospinning. *Advanced Materials* **2003,** *15*, 1929-1932.

30.   Yu, J. H.; Fridrikh, S. V.; Rugtledge, G. C., Production of submicrometer diameter fibers by two-fluid electrospinning. *Advanced Materials* **2004,** *16*, 1562-1566.

31.   Kriel, H. Polylactic acid core-shell fibres by coaxial electrospinning. Stellenbosch University, Stellenbosch, 2010. MSc

32.   Shenoy, S. L.; Bates, W. D.; Frisch, H. L.; Wnek, G. E., Role of chain entanglements on fiber formation during electrospinning of polymer solutions: good solvent, non-specific polymer–polymer interaction limit. *Polymer* **2005,** *46*, 3372-3384.

33.   McCann, J. T.; Marquez, M.; Xia, Y., Melt Coaxial Electrospinning: A versatile method for the encapsulation of solid materials and fabrication of phase change nanofibers. *Nano Letters* **2006,** *6*, 2868-2872.

34.   Sun, B.; Duan, B.; Yuan, X., Preparation of core/shell PVP/PLA ultrafine fibers by coaxial electrospinning. *Journal of Applied Polymer Science* **2006,** *102*, 39-45.

35.   Zhang, Y.; Huang, Z.-M.; Xu, X.; Lim, C. T.; Ramakrishna, S., Preparation of core-shell structured PCL-r-Gelatin bi-component nanofibers by coaxial electrospinning. *Chemistry of Materials* **2004,** *16*, 3406-3409.

36.   Jiang, H.; Hu, Y.; Zhao, P.; Li, Y.; Zhu, K., Modulation of protein release from biodegradable core–shell structured fibers prepared by coaxial electrospinning. *Applied Biomaterials* **2006,** *79*, 50-57.

37.   Wang, M.; Jing, N.; Su, C. B.; Kameoka, J.; Chou, C.-K.; Hung, M.-C.; Chang, K.-A., Electrospinning of silica nanochannels for single molecule detection. *Applied Physics Letters* **2006,** *88*, 033106.

38.   S, M.; JS, S.; DB, C.; JF, R., Micro- and nanostructured surface morphology on electrospun polymer fibers. *Macromolecules* **2002,** *35*, 8456-8466.

39.   Subbiah, T.; Bhat, G. S.; Tock, R. W.; Parameswaran, S.; Ramkumar, S. S., Electrospinning of nanofibers. *Journal of Applied Polymer Science* **2005,** *96*, 557-569.

40.   Larsen, G.; Spretz, R.; Velarde-Ortiz, R., Use of coaxial gas jackets to stabilize Taylor cones of volatile solutions and to induce particle-to-fiber transitions. *Advanced Materials* **2004,** *16*, 166-169.

41.   Reneker, D. H.; Chun, I., Nanometre diameter fibres of polymer, produced by electrospinning. *Nanotechnology* **1996,** *7*, 216-223.

42.   López-Herrera, J. M.; Barrero, A.; López, A.; Loscertales, I. G.; Márquez, M., Coaxial jets generated from electrified Taylor cones. Scaling laws. *Journal of Aerosol Science* **2003,** *34*, 535-552.

43.   Tan, S. H.; Inai, R.; Kotaki, M.; Ramakrishna, S., Systematic parameter study for ultra-fine fiber fabrication via electrospinning process. *Polymer* **2005,** *46*, 6128-6134.

44.   Zeng, J.; Chen, X.; Xu, X.; Liang, Q.; Bian, X.; Yang, L.; Jing, X., Ultrafine fibers electrospun from biodegradable polymers. *Applied Polymer Science* **2002,** *89*, 1085-1092.

45.   Stranger, J. J. Charge transfer mechanisms in electrospinning. University of Canterbury, Canterbury, 2008. MSc

46.   Reneker, D. H.; Yarin, A. L., Electrospinning jets and polymer nanofibers. *Polymer* **2008,** *49*, 2387-2425.

47.   Theron, S. A.; Zussman, E.; Yarin, A. L., Experimental investigation of the governing parameters in the electrospinning of polymer solutions. *Polymer* **2004,** *45*, 2017-2030.

48.   Moghbeli, M. R.; Mohammadi, N.; Bagheri, R.; Ghaffarian, S. R., Wet spinning of low gel content SBR/PMMA core/shell particles dispersed in a good solvent for the shell. *Polymer* **2003,** *44*, 4011-4019.

49.   Teo, W. E.; Ramakrishna, S., A review on electrospinning design and nanofibre assemblies. *Nanotechnology* **2006,** *17*, R89-R106.

50.   Kessick, R.; Fenn, J.; Tepper, G., The use of AC potentials in electrospraying and electrospinning processes. *Polymer* **2004,** *45*, 2981-2984.

51.   Kalayci, V. E.; Patra, P. K.; Kim, Y. K.; Ugbolue, S. C.; Warner, S. B., Charge consequences in electrospun polyacrylonitrile (PAN) nanofibers. *Polymer* **2005,** *46*, 7191-7200.

52.   Katti, D. S.; Robinson, K. W.; Ko, F. K.; Laurencin, C. T., Bioresorbable nanofiber-based systems for wound healing and drug delivery: Optimization of fabrication parameters. *Journal of Biomedical Materials Research* **2004,** *70*, 286-296.

53.   Reznik, S. N.; Yarin, A. L.; Zussman, E.; Bercovici, L., Evolution of a compound droplet attached to a core-shell nozzle under the action of a strong electric field. *Physics of Fluids* **2006,** *18*, 62-101.

54.   Bazilevsky, A. V.; Yarin, A. L.; Megaridis, C. M., Co-electrospinning of core-shell fibers using a single-nozzle **2007,** *23*, 2311-2314.

55.   Smit, E.; Bűttner, U.; Sanderson, R. D., Continuous yarns from electrospun fibers. *Polymer* **2005,** *46*, 2419-2423.

56.   Zhnag, S. Mechanical and physical properties of electrospun nanofibers. North Carolina State University, 2009. MSc

57.   Casper, C. L.; Stephens, J. S.; Tassi, N. G.; Chase, D. B.; Rabolt, J. F., Controlling surface morphology of electrospun polystyrene fibers:Effect of humidity and molecular weight in the electrospinning process. *Macromolecules* **2004,** *37*, 573-578.

58.   Doshi, J.; Reneker, D. H., Electrospinning process and applications of electrospun fibers. *Journal of Electrostatics* **1995,** *35*, 151-160.

59.   Srinivasarao, M.; Collings, D.; Philips, A.; Patel, S., Three-dimensionally ordered array of air bubbles in a polymer film. *Science* **2001,** *292*, 79-83.

60.   Wang, X.; Um, I. C.; Fang, D.; Okamoto, A.; Hsiao, B. S.; Chu, B., Formation of water-resistant hyaluronic acid nanofibers by blowing-assisted electro-spinning and non-toxic post treatments. *Polymer* **2005,** *46*, 4853-4867.

61.   Tokiwa, Y.; Calabia, B. P.; Ugwu, C. U.; Aiba, S., Biodegradability of plastics. International journal of molecular sciences **2009,** *10*, 3722-42.

62.   Chonde, C. S.; Chonde,S. G.; Raut, P. D., Studies on degradation of synthetic polymer nylon 6 and nylon 6, 6 by Pseudomonas aeruginosa. *International Journal of Emerging Technologies in Computational and Applied Sciences* **2013,** *4*, 362-369.

63.   Bshena, O. E. S. Synthesis of permanent non-leaching antimicrobial polymer nanofibers. University of Stellenbosch, Stellenbosch, 2012. PhD

64.   Ikladious, N. E.; Asaad, J. N.; Emira, H. S.; Mansour, S. H., Alkyd resins based on hyperbranched polyesters and PET waste for coating applications. *Progress in Organic Coatings* **2016**, 1-8.

65.   Brasjen, B. J.; Wedershoven, H. M. J. M.; van Cuijk, A. W.; Darhuber, A. A., Dip- and die-coating of hydrophilic squares on flat, hydrophobic substrates. *Chemical Engineering Science* **2017,** *158*, 340-348.

66.   Licari, J. J., In *Coating Materials for Electronic Applications*, William Andrew Publishing: Norwich, NY, 2003.

67.   Mishra, S. K.; Kumar, V.; Tiwari, S. K.; Mishra, T.; Angula, G.; Adhikari, S., Development and degradation behavior of protective multilayer coatings for aluminum reflectors for solar thermal applications. *Thin Solid Films* **2016,** *619*, 202-207.

68.   Scriven, L. E., Physics and applications of DIP coating and spin coating. *MRS Proceedings* **1988,** *121*.

69.   Rahaman, M. N., Ceramic processing. *CRC Press* **2007**, 242-244.

CHAPTER 3

Experimental

3.1   Modification of SMA with *N*,*N*-dimethyl-3-aminopropyl-1-amine

This chapter describes the experimental procedures and protocols used for the preparation of SMI-P as well as the characterization. Commercial poly(styrene-*co*-maleic anhydride) grade was used.

3.1.1   Materials

The materials that were used in the synthesis of SMI-P were as follows: poly(styrene-*co*-maleic anhydride) (SMA-C) which was a commercial grade with an M_w = 120 000 g/mol containing about 26 wt% maleic anhydride (MAnh) moieties as a statistical copolymer obtained from Polyscope, grade SZ 26 120. The chemicals used were *N*,*N*-dimethyl-3-aminopropyl-1-amine (DMAPA) 99% (Aldrich), tetrahydrofuran (THF) 99% (Aldrich), *N*,*N*-dimethylformamide (DMF). The other chemicals that were used for the electrospinning solutions were ethanol (99%) (Aldrich) and formic acid (99%) (Aldrich) and the nylon 6 that was used was obtained from BDH Laboratory Reagents.

3.1.2   Synthesis of poly(styrene-*co*-*N*-(*N'*,*N'*-dimethyl-3-aminopropyl)maleimide)

Poly(styrene-*co*-maleic anhydride) (15 g, 40 mmol MAnh residues) and DMF (75 mL) were placed in a 250 mL round bottom flask and stirred to dissolve the polymer. *N*,*N*-dimethyl-3-aminopropyl-1-amine (9.9 g, 97 mmol) was placed in a dropping funnel and added to the solution dropwise over a period of 15 minutes. The reaction solution was heated to 170 °C and refluxed for 1 hour. Subsequently, the solution was allowed to cool and the polymer was precipitated in water and filtered off. The precipitate was placed in a vacuum oven at 60 °C for 24 h. **Figure 3.1** shows the scheme of the polymer synthesis.
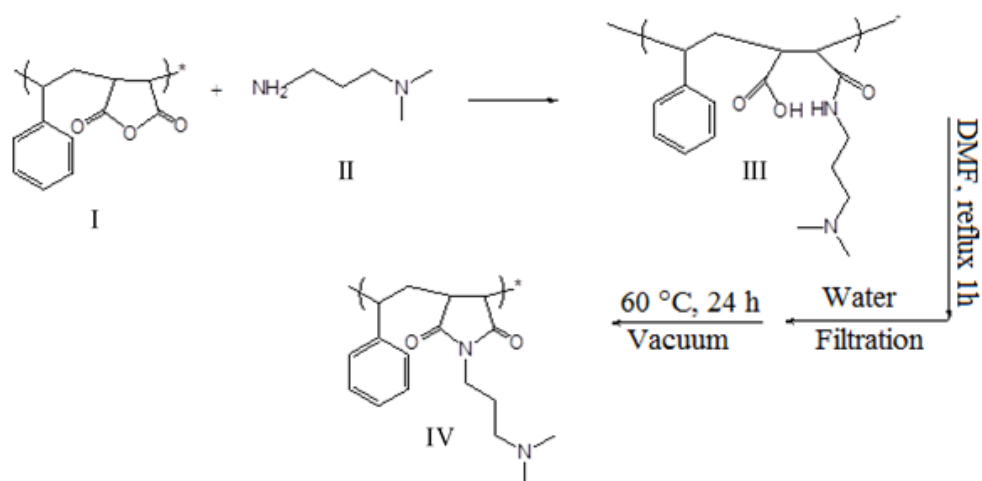
Figure 3.1: Imidization and ring closure of the SMA to SMI-P

3.1.3   Synthesis of poly(styrene-*co*-N-(*N'*, *N'*-dimethyl-3-aminopropyl) maleimide) with lower targeted MAnh conversion

There were two polymers made by targeting a lower fraction of MAnh (I) to be converted and they are the 70% SMI-P and 90% SMI-P. The 70% SMI-P was synthesised the same as the fully converted SMI-P (IV) as shown in Section 3.1.2 except that the amount of DMAPA (II) used was reduced to 2.84 g (28 mmol). The 90% SMI-P was produced the same way as SMI-P as shown in **Section 3.1.2** except the DMAPA that was added was reduced to 3.66 g (36 mmol).

3.2   Labelling process

The labelling of the SMI-P nanofibres was done as shown in **Figure 3.2**. As illustrated in the scheme, 6-aminofluorescein (V) can only be attached to the maleic anhydride group and cannot be attached to SMI-P (IV). It is for this reason that the SMI-P that was used for the fluorescence imaging had to contain some unconverted MAnh moieties, hence the 70% converted and 90% converted SMI-P. For the fluorescent labelling, 0.5 g

6-aminofluorescein was dissolved in 50 mL water. This was followed by complete submersion of the nanofibre mats in the 6-aminofluorescein solution for 3 hours and finally rinsing of the mats with deionised water and air drying. Some samples were labelled before electrospinning, which was done by dissolving 10 g of the 90% SMI-P and 1 g 6-aminofluorescein in DMF and stirring for 3 hours. The labelled polymer was then precipitated in water and filtered off. The solid labelled polymer was used to make the electrospinning solution instead of the standard polymer.
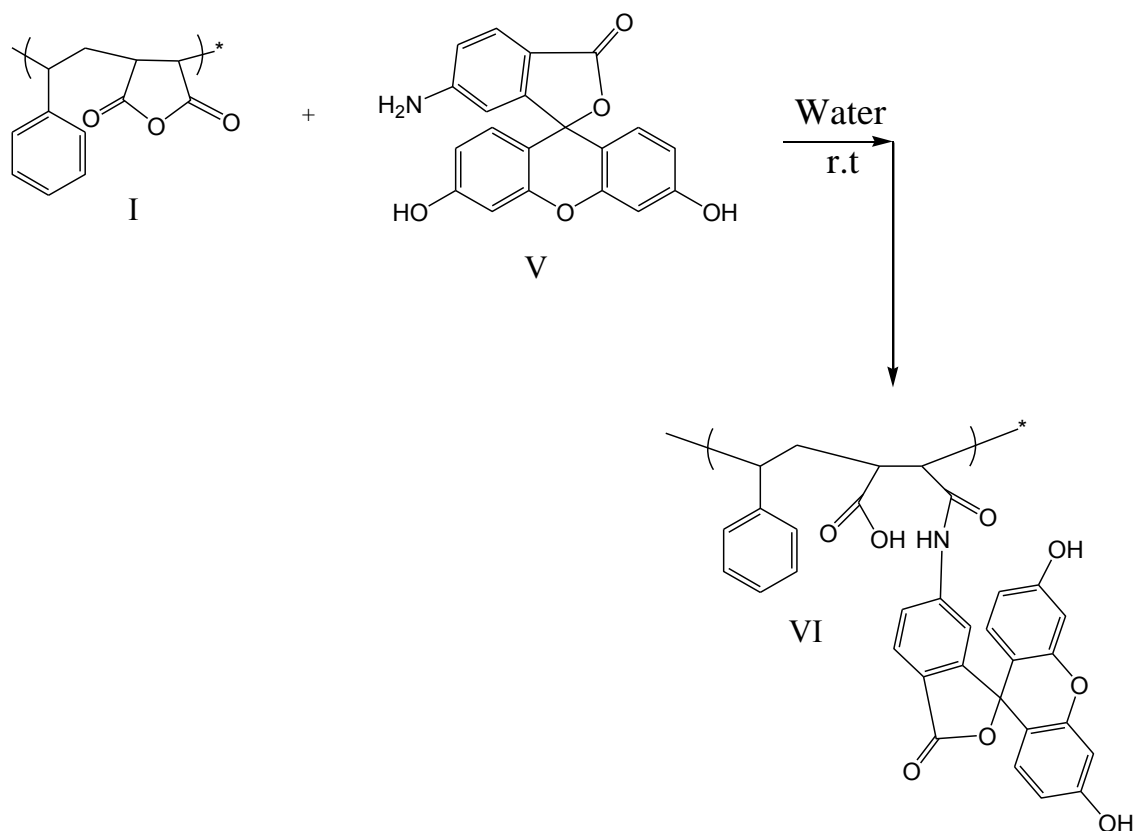
Figure 3.2: Scheme of labelling of SMA with 6-aminofluorescein

3.3   Characterization

3.3.1 Differential scanning calorimetry (DSC)

DSC measurements were performed on a TA Advanced Q1000 calorimeter. The sample runs where done in a three main step process. First the samples were heated from 0 to 200 °C at a rate of 10 °C/min and this was followed by an isothermal step for 1 min. Then a cooling run occurred, which cooled the sample down to 0 °C at 10 °C/min and then a second heating run occurred to heat the sample back up to 200 °C at 10 °C/min.

The glass transition temperature (T_g) was obtained from the second heating run that was performed on the samples.

3.3.2   Fourier transform infrared spectroscopy (FTIR)

Attenuated Total Reflection Fourier Transform Infrared (ATR-FTIR) spectroscopy was carried out on a Nexus infrared spectrometer that was equipped with a smart golden gate attenuated total reflectance diamond from Thermo Nicolet with ZnSe lenses. Every sample was scanned 64 times with 4.0 cm^{-1} resolution. The software that was used on the system to do the data analysis was Omnic Software, version 7.2.

3.3.3   Nuclear magnetic resonance (NMR)

The ^{1}H-NMR measurements were carried out at 50°C on a Varian Mercury 400 MHz or Varian Unity Inova 600 MHz spectrometer in either deuterated dimethyl sulfoxide (DMSO-d6) or deuterated chloroform (CDCl$_3$). Mestranova software version 6.02 was used to view and analyse the NMR data obtained from the spectrometer.

3.4   Single needle electrospinning

3.4.1   Setup

The single needle electrospinning unit that was used was the standard system and as shown in **Figure 3.3**. The system consisted of a Kent Scientific Genie Plus syringe pump, the high voltage power supply and the collector plate. The collector plate consisted of a glass petri dish that was covered with aluminium foil where after the power supply's negative port was connected to the plate and the positive was connected to the needle tip. This system was used to determine the individual polymer solution's parameters to have a starting point for the coaxial electrospinning parameters.
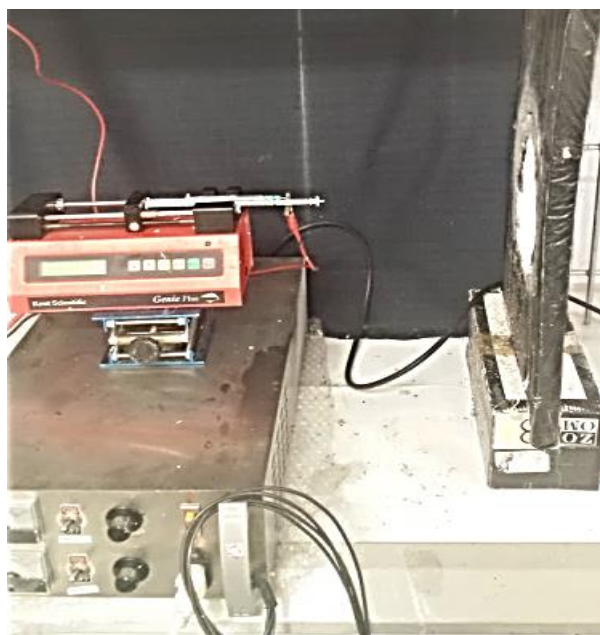
Figure 3.3: Electrospinning setup

3.4.2   Solutions

The polymer solutions for single needle electrospinning were prepared as shown in Table 3.1. SMI-P (1) and SMI-P (2) were made by the method described in Section 3.1.2 and the 90% SMI-P was made as shown in Section 3.1.3. The samples were prepared and allowed to stir overnight in a tightly closed flask (to avoid solvent evaporation) in order to allow for a completely homogeneous solution. Different variations of the solutions were made to optimize the electrospinning process and obtain the best possible fibres. These variations ranged from the solution concentration and adjusting the solvent ratios and the solvents used until the best fibre morphology was obtained.

Table 3.1: Optimized polymer solution compositions

Polymer	Percentage	Solvent	Solvent ratios
SMI-P (1)	18 wt/wt	ethanol : DMF	80:20
SMI-P (2)	18 wt/wt	DMF : THF	50:50
Nylon 6	10 wt/wt	formic acid	-
90% SMI-P	20 wt/wt	DMF	-

3.4.3   Parameters

The electrospinning process was manipulated by adjusting the voltage, spinning distance, flow rate and the type of collector that was used. The final and best parameters that were used are shown in Table 3.2. The use of the drum collector allowed for the elimination of persistent beading.

Table 3.2: Optimized electrospinning parameters for the polymer solutions

Polymer	Voltage (kV)	Distance (cm)	Flow rate (mL/min)	Collector
SMI-P (1)	15	20	0.0033	Stationary
SMI-P (2)	15	20	0.0033	Drum
Nylon 6	15	15	0.0033	Stationary
90% SMI-P	15	20	0.0033	Drum

3.5   Coaxial electrospinning

3.5.1   Setup

The coaxial electrospinning setup looks identical to that of the single needle electrospinning system. The only difference between the two systems is the needle and syringe system that is used. In the coaxial system, a second polymer solution supply is needed to produce the core-shell fibre configuration. The needle and syringe system that was used to attain this configuration can be seen in Figure 3.4. In this setup, two different polymer solutions can be electrospun. The flow rate is adjusted in such a way that it is compatible with both polymer solutions used. From the optimization studies, it was found that, starting with lower flow rates and adjusting accordingly until the optimal rate produced good results.
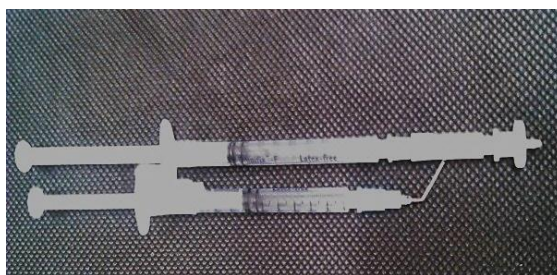
Figure 3.4: Coaxial needle and syringe setup used during coaxial electrospinning

3.5.2   Solutions

The solutions for the coaxial electrospinning system were made by using the optimized solutions that were obtained by the electrospinning of the single polymer solutions and can be seen in Table 3.3. If these solutions do not make the best fibres, then optimization of the solutions can be done. The optimization can be done by altering the solvent and there concentrations.

Table 3.3: Polymer solutions and combinations for coaxial electrospinning

Coaxial layer	Polymer	Percentage	Solvent	Solvent ratios
Shell	SMI-P (1)	18 wt/wt	ethanol : DMF	80:20
Core	Nylon 6	10 wt/wt	formic acid	-
Shell	90% SMI-P	20 wt/wt	DMF	-
Core	Nylon 6	10 wt/wt	formic acid	-

The parameters for the coaxial electrospinning system were taken from the single needle optimization conditions. In the case of the parameters differing between the core and the shell polymer solutions, the lowest flow rate was taken, in the case of the spinning distance, the larger distance was chosen and in the case of the voltage it was adjusted during the electrospinning process. The final parameters are shown in Table 3.4

51

Table 3.4: Optimized coaxial electrospinning parameters for the polymer solutions

Coaxial layer	Polymer	Voltage (kV)	Distance (cm)	Flow rate (mL/min)	Collector
Shell	SMI-P (1)	15	20	0.0033	Stationary or Drum
Core	Nylon 6	15	20	0.0033	
Shell	90% SMI-P	15	20	0.0033	Drum
Core	Nylon 6	15	20	0.0033	

3.6   Coating process

Nylon 6 electrospun nanofibre mats were coated using the polymer compositions in Table 3.5. As it can be noted from the polymers in Table 3.5, different conversions of SMA to SMI-P were used. This was done to allow for chemical bonding of the nylon and SMI-P as well as for fluorescent tagging of the fibres to confirm the coaxial structure. The coating was done using the dip coating method. The samples were dipped into the coating solutions shown in Table 3.5 and once the sample was dipped, it was suspended vertically to allow the sample to dry and excess solution to drip off. The coated samples were then viewed under SEM to make sure that the fibre structure is still intact and that the coating did not produce a film over the nanofibre mat.

Table 3.5: Coating solutions produced

Polymer	Percentage of coating solution	Solvent	Solvent ratios
SMI-P	0.5 wt/wt	Ethanol:DMF	80:20
90% SMI-P	0.5 wt/wt	DMF	-
70% SMI-P	0.5 wt/wt	DMF	-
SMA	0.5 wt/wt	DMF	-

3.7   SEM/STEM

The samples were loaded in a Zeiss MERLIN Field Emission Scanning Electron Microscope at the Electron Microbeam Unit of Stellenbosch University's Central Analytical Facility. Prior to imaging, the samples were mounted on aluminum stubs with double sided carbon tape. The samples were then coated with a thin (~10 nm thick) layer of carbon, using a Quorum carbon coater. This is done to make the sample surface electrically conductive to avoid electron build-up on the sample surface which can cause electron charge.

Scanning electron images of the sample were captured using a Zeiss Secondary Electron (SE2) detector or the Zeiss inlens detector using Zeiss SmartSEM software. The beam conditions during the image analysis were 5 kV acceleration voltage Extra-High Tension (EHT) target, 250 pA beam current (I-Probe), less than 4 mm working distance (WD) and a high resolution column configuration (Column Mode).

The scanning transmission electron microscope (STEM) images were acquired using the Zeiss MERLIN Field Emission Scanning Electron Microscope at the Electron Microbeam Unit of Stellenbosch University's Central Analytical Facility. Prior to loading the samples into the microscope, the sample solution was electrospun onto copper transmission electron microscope (TEM) grids. The TEM grid was loaded into the 12-place STEM sample holder and fastened into place with a copper ring and screw. A Zeiss five-diode Scanning Transmission Electron Detector (Zeiss aSTEMA Detector) and Zeiss Smart SEM software were used to generate STEM images. Beam conditions during analysis on the Zeiss MERLIN FE-SEM were 20 kV accelerating voltage, 250 pA probe current, with a working distance of approximately 4 mm, and an analytical column configuration (column Mode). Images were acquired in bright field mode with the S1 diode activated.

3.8   Fluorescence microscopy

The samples that were tagged with a fluorescent label were imaged using the ZEISS LSM 780 confocal microscope with ZEN 2012 software for recording the fluorescence of the images. The laser that was used was the 488 nm laser that was used for excitation and the emission was detected in the 490-570 nm range. The samples were tagged with

6-aminofluorescein as the fluorescent label. The sample images were acquired at 10x/0.30 and 100x/1.46 Oil magnification.

3.9   Dissolution test

Dissolution tests were carried out to remove the SMI-P shell of the coaxial electrospun nanofibres. This was done to prove that the shell was SMI-P and that the core was nylon 6. To do this, electrospun coaxial nanofibre mats were submerged in DMF for a week to remove the SMI-P shell from the sample (SMI-P dissolves in DMF and nylon 6 does not). The DMF was changed every second day and after the week, the sample was removed and allowed to dry. This was done on both the standard coaxial electrospun sample and for the labelled coaxial sample. The labelled sample was first imaged with the confocal microscope and then again after the dissolution was done and the same was done for the standard sample except the imaging was done on the EM and the fibre diameter was measured with Axiovision software to see if the shell layer was removed.

3.10   Antimicrobial tests

3.10.1 Zone inhibition method

Antimicrobial tests were carried out on the bacteria as shown in Table 3.6. The plates were first prepared with a growth medium; Mueller-Hinton agar (composition - g/L: meat infusion (5.0), casein hydrolysate (17.5), soluble starch (1.5), agar (14.0)) obtained from Biolab Diagnostics (Pty) Ltd was made as instructed on the container and was then autoclaved. Then after the autoclaving the solution was left to cool till the container could be handled. The Mueller-Hinton agar was then poured into the plates up to the designated points and was left to solidify overnight. Nutrient broth (composition - g/L: meat extract (1.0), yeast extract (2.0), peptone (8.0)) obtained from Biolab Diagnostics (Pty) Ltd was then made as instructed on the container. The broth mixture (10 mL) was added to 12 test tubes to run the test in duplicate and this is then autoclaved. Then once this has cooled down completely the bacteria were transferred to each test tube by collecting a bacteria colony in a plastic syringe tip and placing it in the broth. The test tubes with the bacteria were then put on a rotating incubator at 37 °C for 24 hours. This was followed by the transfer of the bacteria to the plates and 10 µL of the broth/bacteria was added to each plate and spread to form a lawn. The plates were divided into four

quarters and the samples were placed in different quarters and were placed in the oven for 24 hours at 37 °C. Then the samples were checked for antimicrobial activity after that. The activity was checked by observing if there was a clearing around the samples and then the diameters of the clearings were measured and compared to the standards to obtain if the antimicrobial activity remained constant for all the samples.

Table 3.6: Bacteria that were used in the disk diffusion method

Gram Status	Bacteria Name	Sample number	Abbreviated Name
+	*Staphylococcus aureus*	ATCC 25925	*S.aureus*
-	*Salmonella typhi*	ATCC	*S.typhi*
-	*Pseudomonas aeruginosa*	ATCC 27853	*P.aeruginosa*
-	*Escherichia coli*	ATCC 13706	*E.coli*
+	*methicillin-resistant Staphylococcus aureus*	Xeu 36	*MRSA*
+	*Bacillus subtilis*	ATCC 6051	*B.subtilis*

3.10.2 Live/Dead fluorescence

The bacteria in Table 3.7 were streaked out onto Luria Bertani broth (LB) agar (1.5% agar) plates and were grown overnight at 37 °C. Then 3-5 colonies were inoculated into 20 mL of clean LB medium (1% tryptone, 1% NaCl, 0.5% yeast extract) and were grown overnight at an angle rotating at 150 RPM at 37 °C. The cultures were diluted to an $OD_{620} = 0.2$ and then 5 µL of the diluted cultures were transferred onto each sample. Then the samples were taken for fluorescence imaging where the samples were each stained with both propidium iodide and SYTO 9 dye and 15 minutes later the imaging was started. The same instrumentation was used as for the fluorescence imaging in **Section 3.8**. The emission from the dyes was at 561 nm for the red fluorescence and 488 nm for the green fluorescence. The images were taken 15 minutes after the staining with the dyes occurred and then again 24 hours later again to observe whether the bacteria were killed. In the case of the bacteria being alive the bacteria produce green fluorescence and once the bacteria die it produces red fluorescence.

Table 3.7: Bacteria used in the live/dead fluorescence method

Gram Status	Bacteria Name	Sample number	Shorted Name
+	*Staphylococcus aureus*	ATCC 25925	*S.aureus*
-	*Pseudomonas aeruginosa*	ATCC 27853	*P.aeruginosa*

CHAPTER 4

Results and discussion

This chapter outlines findings of the study and either supports or refutes them based on relevant literature. Results on the characterization of the polymers before and after the electrospinning or coating processes and the morphology of the fibres are discussed in this chapter. Additionally, chemical, antimicrobial and mechanical results are reported and discussed.

4.1   Polymer characterization results and discussion

In this section, details on the characterisation of the pristine polymers used in this study are reported and discussed.

4.1.1   Poly(styrene-*co*-*N*-(*N'*,*N'*-dimethyl-3-aminopropyl)maleimide)

4.1.1.1 ATR-FTIR spectroscopy

ATR-FTIR was used to characterize the synthesized poly(styrene-*co*-*N*-(*N'*,*N'*-dimethyl-3-aminopropyl)maleimide). In **Figure 4.1**, the ATR-FTIR spectra of SMA (top) and SMI-P (bottom) are shown. The bands at about 1855 and 1770 cm^{-1} are characteristic of asymmetric and symmetric C=O stretching vibrations from the anhydride groups. The bands at about 1605 and 1500 cm^{-1} are from C=C stretching of the aromatic ring and C-H bending vibrations of the aromatic ring respectively. Then the bands at about 916, 1078 and 1220 cm^{-1} are from the cyclic anhydride groups. The imidization from SMA to SMI-P was confirmed from the observed shift of the C=O carbonyl anhydride peaks to 1770 and 1689 cm^{-1}.[1]
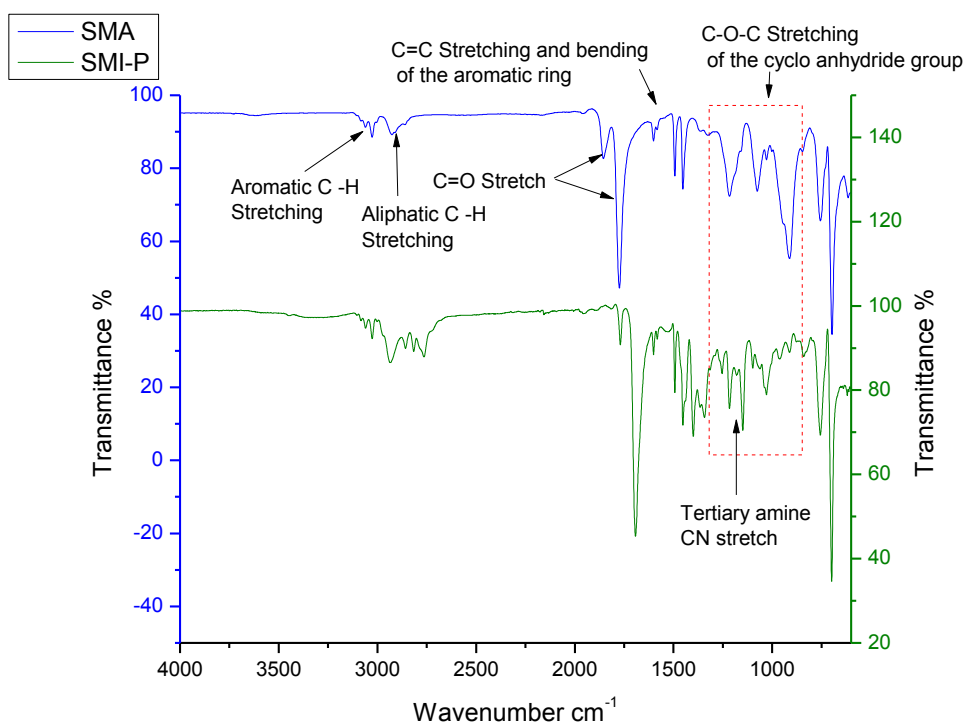
Figure 3.1: ATR–FTIR spectra of SMI-P (green) and SMA (blue)

4.1.1.2 Nuclear magnetic resonance (NMR)

The ^{1}H-NMR spectrum in Figure 4.2, is indicative of the polymer modification. This is evidenced by the broad peaks. The peaks between 6.7-7.5 ppm and 3.3 ppm, correspond to the protons on the aromatic ring (c) and methine protons on the SMA polymer backbone (a,a[1]) respectively. The peak at 1.7 ppm is characteristic of the methylene protons (h) on the propyl chain, whereas the peak at 2.17 ppm corresponds to the methyl protons (e) and methylene protons (g) adjacent to the tertiary amine. The (g) protons are more downfield from the other methylene protons (h) due to the deshielding effect of the electronegative character of nitrogen of the tertiary amine. The (f) methylene protons that are adjacent to the imide nitrogen are also affected by the deshielding effect and so gets shifted downfield to overlap with the methine protons of the maleic anhydride unit. Figure 4.2 clearly shows that a polymer was formed, and the few solvent impurities present are very little to cause any problems during electrospinning. Figure 4.2 along with Figure 4.1 clearly shows that SMI-P was synthesised.[2]
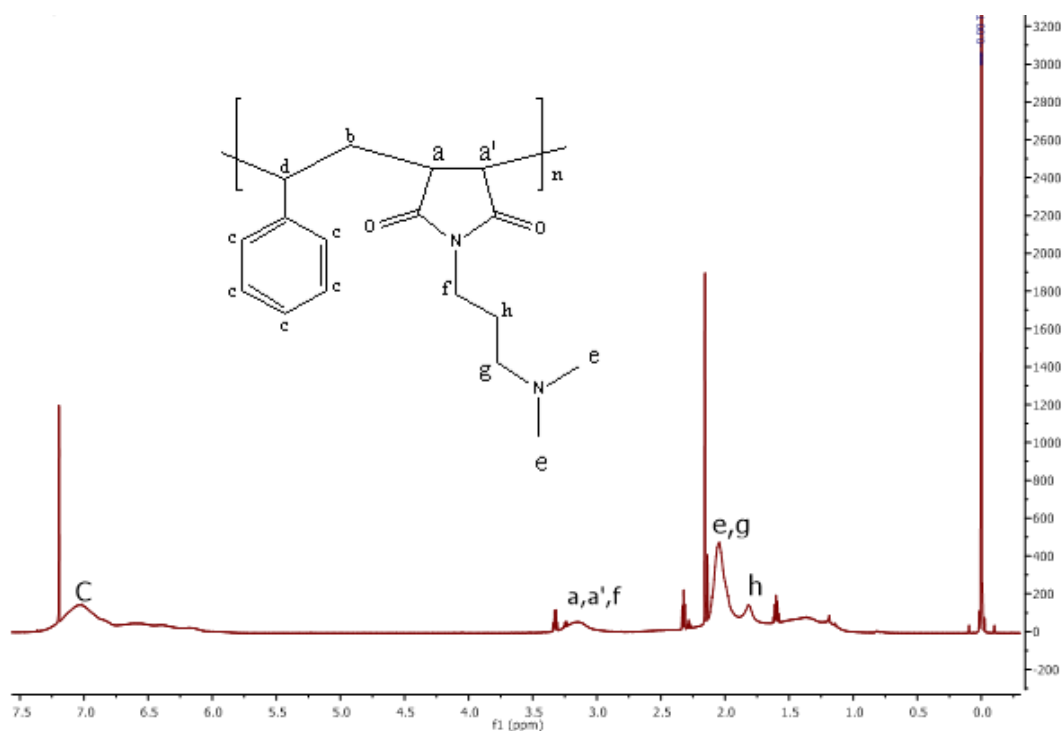
Figure 3.2: ^{1}H-NMR spectrum of SMI-P in CDCl₃

4.1.1.3 Differential scanning calorimetry (DSC)

Differential scanning calorimetry was performed to further confirm the formation of SMI-P from SMA. A three-cycle process from 0 °C to 200 °C was adopted. The thermogram from the third cycle, which indicates the T_g of SMI-P is shown in Figure 4.3. According to literature, SMI-P with a similar composition to the polymer used in this study has a T_g of about 123 °C, but due to the T_g being influenced by the polymer composition the obtained T_g for SMI-P is expected to be slightly different than that found in literature. The results obtained for the SMI-P synthesized in this study was in the same region as literature as seen on the thermogram in Figure 4.3. SMA has a T_g of 160 °C and a clear decrease in the T_g is seen due to the imidization that occurred. This decrease in T_g as well as FTIR and ^{1}H-NMR results all confirm a successful synthesis of SMI-P.[1]
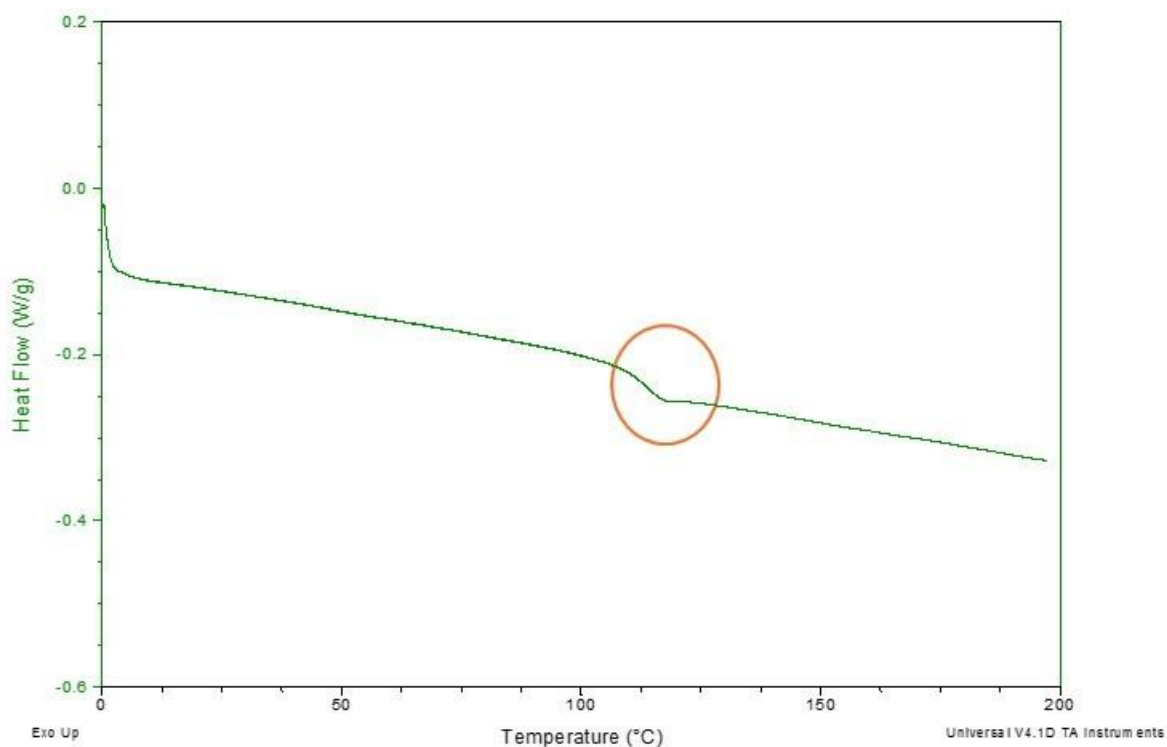
59

Figure 3.3: DSC thermogram of SMI-P

4.2   Characterization of pristine nylon 6

For conclusions to be drawn on the coaxial fibres, it was necessary for nylon fibres to be characterized as well to pick up any changes the presence of nylon-6 would bring to the final product. FTIR and DSC analysis were conducted on this polymer.

4.2.1 ATR-FTIR spectroscopy

In Figure 4.4, the ATR-FTIR spectra of nylon 6 is shown. The bands at 1600 cm^{-1} and 1500 cm^{-1} are due to the carbonyl (-C=O) as well as the N-H bending vibrations respectively. The C-H bonds in the nylon 6 are shown by the bands at 2900 cm^{-1} and the N-H stretching vibrations band is seen at 3300 cm^{-1}. This is in line with what is reported in literature.[3]
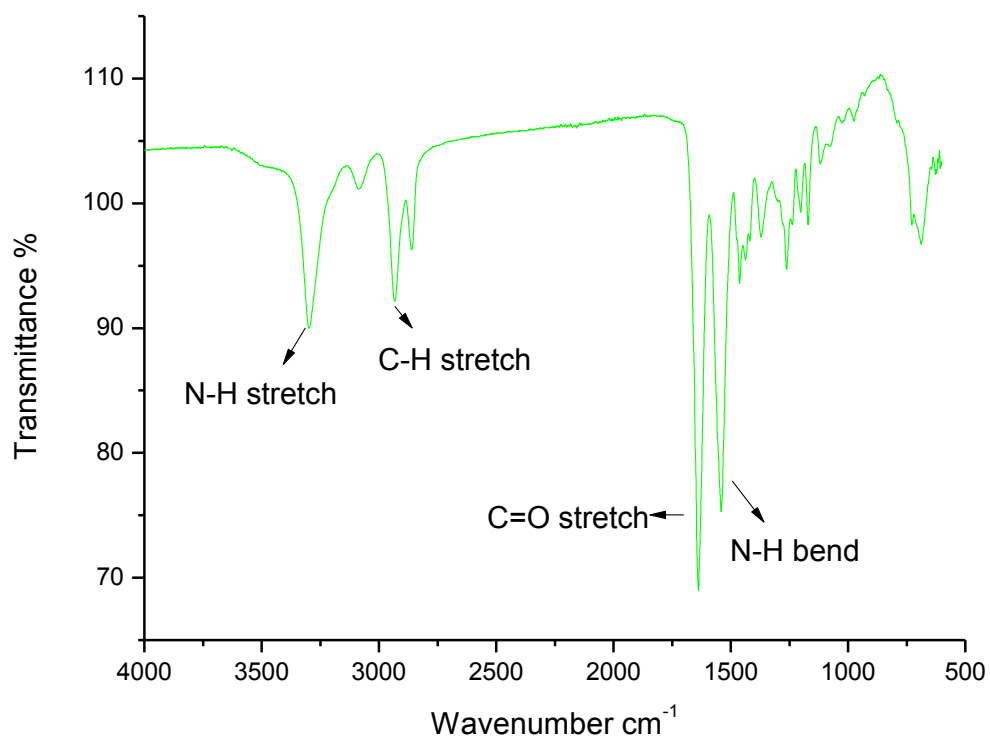
Figure 3.4: ATR–FTIR spectra of nylon 6

4.2.2 Differential scanning calorimetry

The DSC curve shown in Figure 4.5 is of nylon 6 and from the thermogram, the T_g of nylon was around 49 °C which matches well with the literature T_g value of around 50 °C.[4]
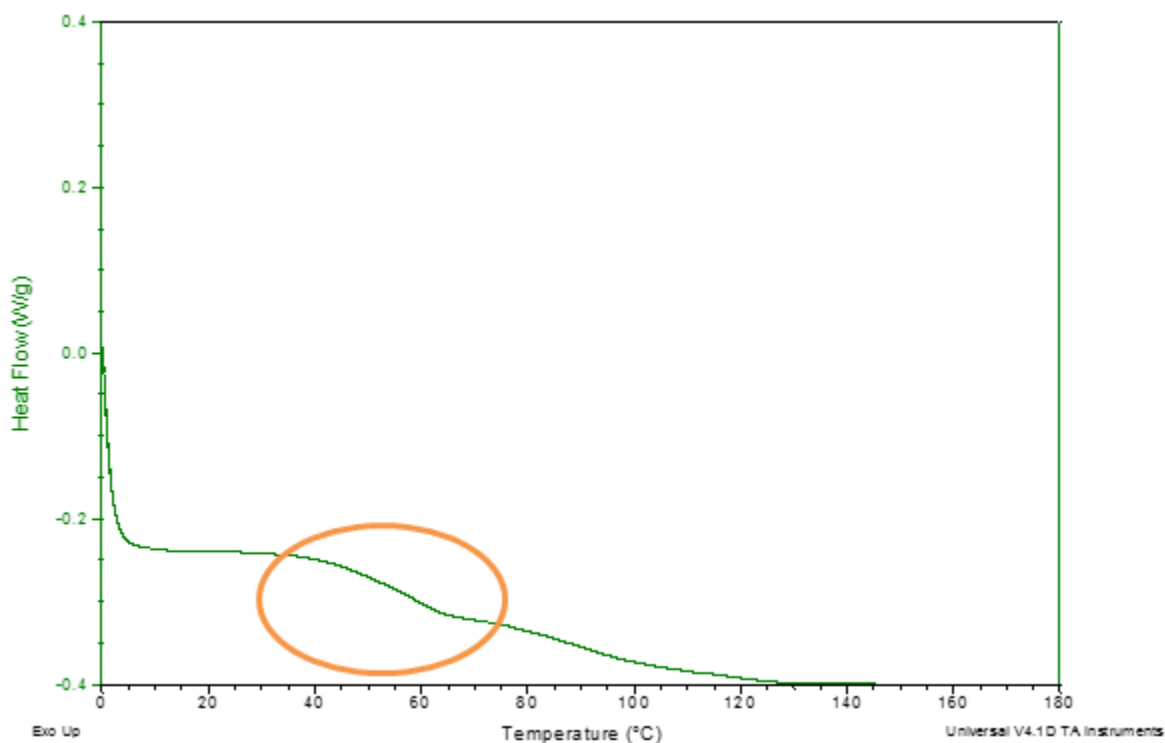
Figure 3.5: DSC curve of nylon 6

4.3 **Coaxial fibres**

The polymers described in Section 3.1.2 and 4.1 were used to fabricate coaxial nanofibers. The core of the fibres was nylon 6 and the shell SMI-P. These coaxial nanofibers were fabricated via two ways; which were coaxial electrospinning and coating. The next few sections will discuss the fibre characteristics of the fibres obtained.

4.3.1 **Fibres obtained via coaxial electrospinning**

After successful optimization of the electrospinning technique for the electrospinning of SMIP-co-nylon 6 fibres the fibre where observed using Scanning electron microscopy. SEM was carried out to determine the morphology of the fabricated fibres. The SEM images in Figure 4.6 show the optimised electrospun nanofibers of nylon 6 (A), pristine SMI-P (B, C) and the coaxial fibres (D). The SMI-P fibres where electrospun with different solvents and images B and C are the best fibres obtained. The solvent compositions used during electrospinning can be seen in Table 3.1 on page 41. The coaxial electrospun fibres (D) were uniform without any beading. SEM however, only

shows that fibres were formed during the electrospinning process and no information about the coaxial structure can be obtained from these images. Thus, the coaxial nanofibers required further analysis to prove that the core-shell morphology was achieved.
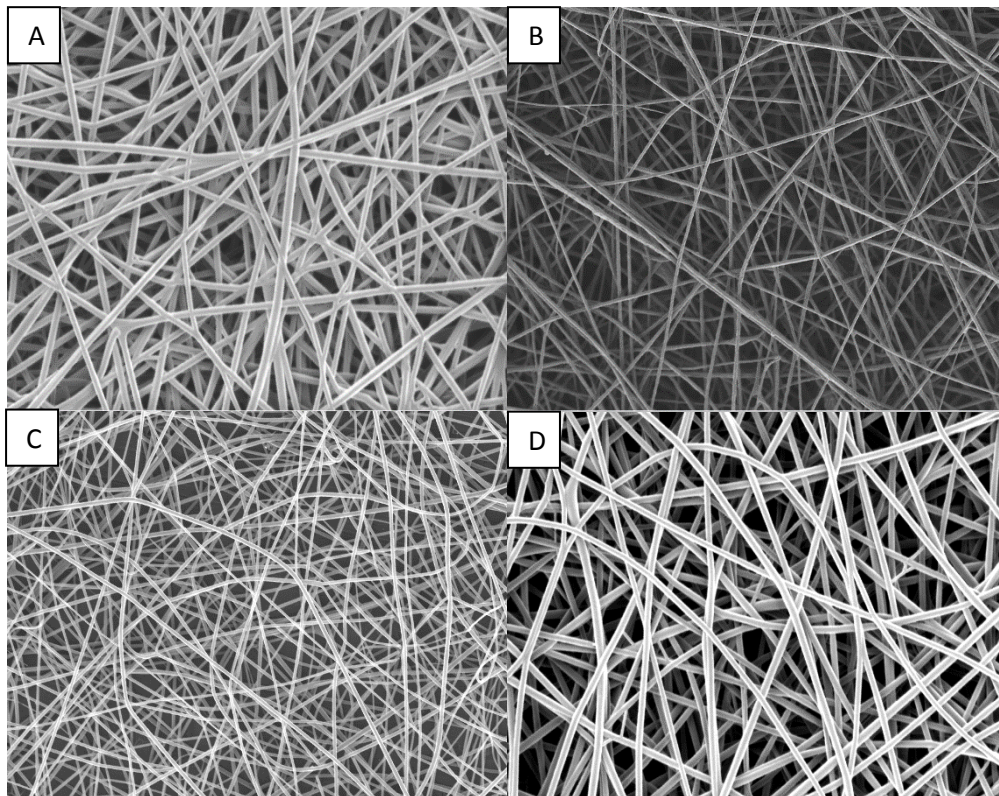

Figure 3.6: SEM images of nylon 6 (A), SMI-P 1 (B), SMI-P 2 (C) and coaxial nanofibers (D)

4.3.2 Confirmation of coaxial nature of the fibres

This section reports on the results of the tests carried out to confirm that the core-shell structured fibres were indeed produced.

4.3.2.1 Scanning transmission electron microscopy (STEM)

Scanning transmission electron microscopy was used to visualize the core shell morphology of the nanofibres. The STEM images in Figure 4.7 show the coaxial electrospun nanofibers and the individual polymer fibres of the polymers that make up the coaxial fibres. It can be seen from the STEM image of pure SMI-P which comes up as white fibres (A) and no core is present in the fibres. The coaxial fibres' STEM images (C, D) with the uranyl acetate added to the nylon 6 core shows that the fibre does have the core-shell morphology as the core can be visualised in the STEM images. Uranyl

acetate was added to the electrospinning solutions to ensure that the nylon can stand out as the core on coaxial nanofibers. In scanning transmission microscopy, it is possible to observe false core-shell morphology. This comes as a result of the fibres being thinner at the sides than the core and this could make the fibres appear as core-shell fibres when they are not. From the results obtained, the nylon 6 with uranyl acetate was evaluated under the STEM and the same structure is not present, but a dark singular fibre is observed. Then the nylon 6 fibre image (B) and the pure SMI-P (A) fibres do not have such an artefact (false core-shell) and only the coaxial fibres possess the co-shell structure (C, D). This was a good indication that it was in fact the real structure and not just an artefact.
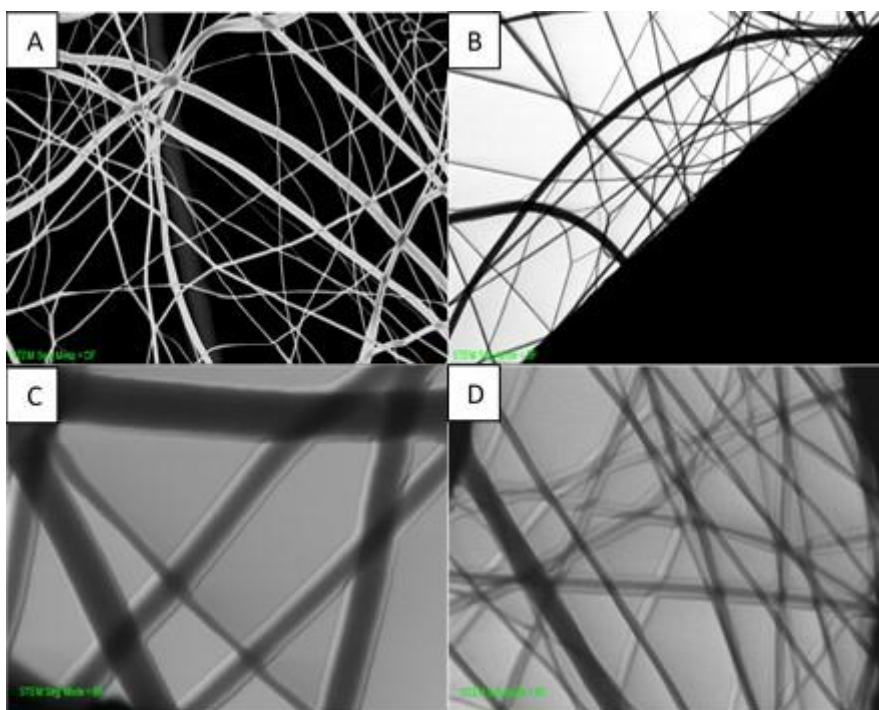

Figure 3.7: STEM images of SMI-P fibres (A), nylon 6 with uranyl acetate (B) and coaxial fibres with the nylon 6 and uranyl acetate in the core (C, D*)*

4.3.2.2 ATR-FTIR spectroscopy

To further confirm the successful formation of coaxial nanofibers via electrospinning, ATR-FTIR analysis was carried out on the fibre mats. In Figure 4.8, the ATR-FTIR spectra of the coaxial nanofibers. The presence of the C=O bands at 1770 and 1689 cm^{-1} in the spectrum indicates the presence of the SMI-P as these bands are characteristic of SMI-P. The spectrum shows the bands that are characteristic for nylon 6 at 1600 cm^{-1}

and 1500 cm^{-1} that are due to the carbonyl (-C=O) as well as the N-H bending vibrations respectively. The C-H bonds in the nylon 6 are shown by the bands at 2900 cm^{-1} and the N-H stretching vibrations band is seen at 3300 cm^{-1}. Thus, with both the bands of nylon 6 and the C=O bands of SMI-P it can be concluded that both polymers are present in the coaxial electrospun mat. Thus the FTIR only proves that both polymers are present in the sample and does not prove the core-shell structure.
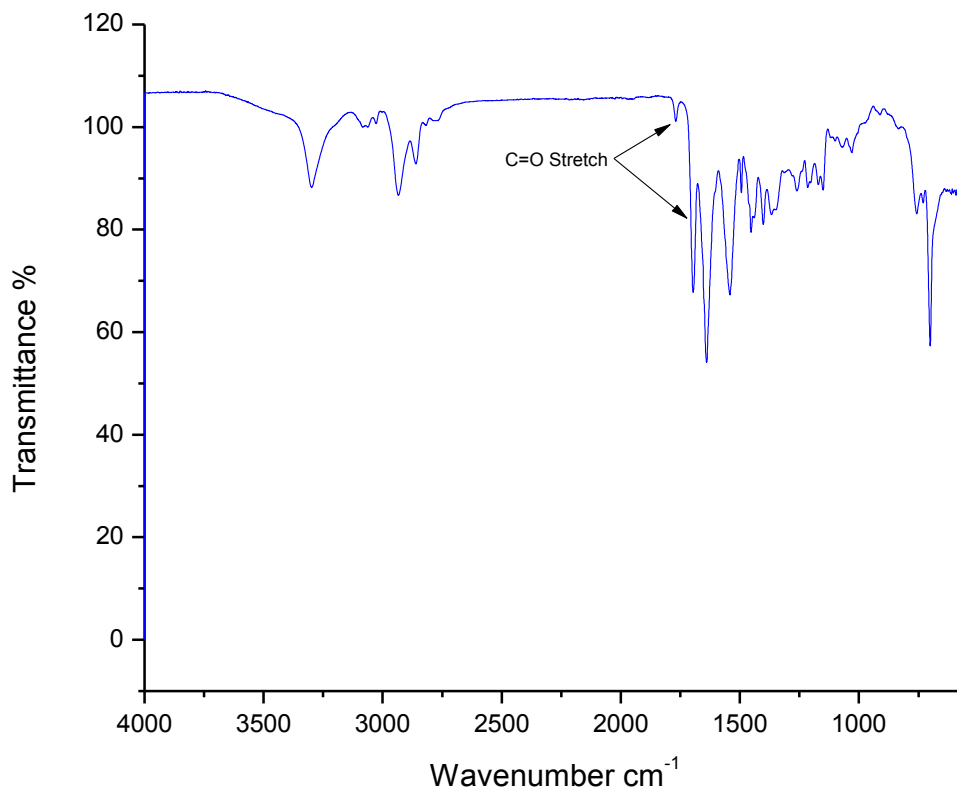

Figure 3.8: ATR–FTIR spectra of the coaxial nanofibers

4.3.2.3 Differential scanning calorimetry

Figure 4.9 shows DSC results of the coaxial electrospun nonofibre mat. The thermogram shows a T_g at around 115 °C and another at around 50 °C. The two T_gs that are observed are at roughly the same temperatures as that of SMI-P and nylon 6 individually. The fact that the T_g values stay the same as for the polymers individually and no new T_g is formed

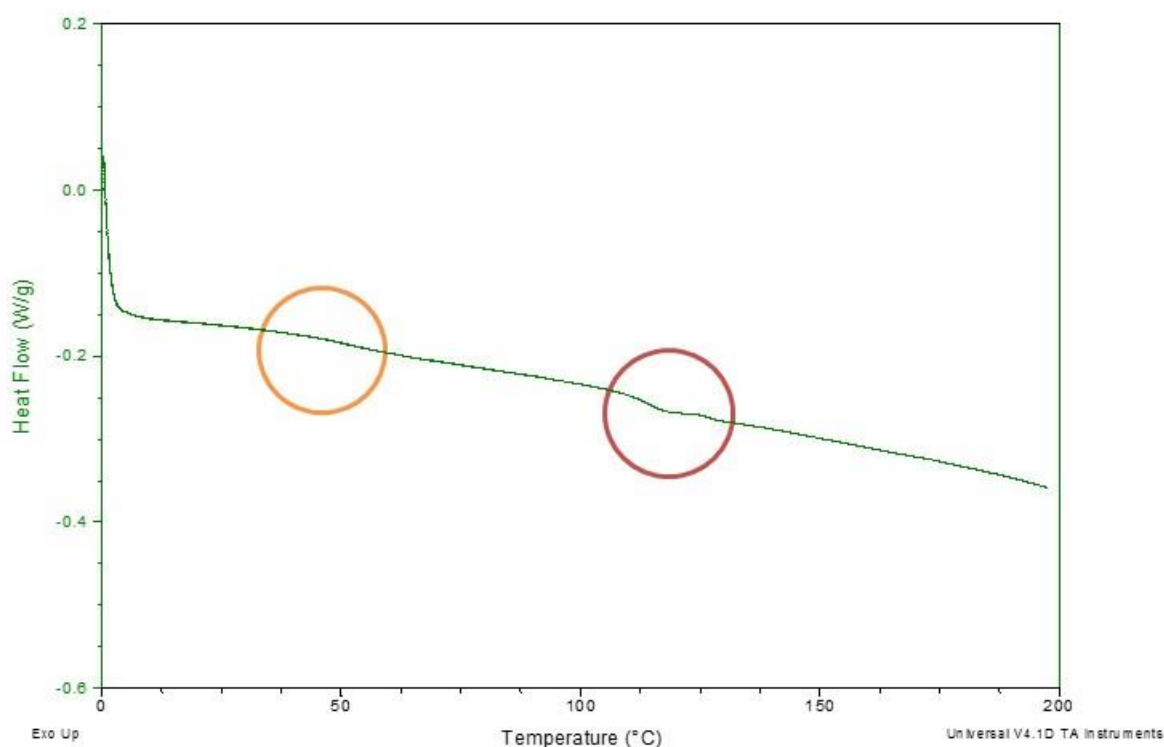indicates that the nylon 6 and SMI-P are immiscible which is a requirement for co-axial electrospinning.

Figure 3.9: DSC curve of the coaxial nanofibers

4.3.2.4 Dissolution tests

SMI-P is soluble in dimethyl formamide (DMF) while nylon-6 is not. The coaxial nanofiber mats were exposed to DMF in order to dissolve the SMI-P and hence prove that there was nylon-6 on the core of the fibres. The SEM images in Figure 4.10 shows the coaxial nanofibers (A) prior to being exposed to DMF along with the image used for the diameter measurements of the coaxial fibres (B). Figures 4.10 C and D are the fibres after the SMI-P was dissolved. The fibre diameters were measured and recorded as shown by Table 4.1. The coaxial fibre diameters were measured before the shell was dissolved and the fibres were found to have an average diameter of 0.111 μm. After the shell was dissolved, the fibres were measured again and it was found that the average fibre diameter was 0.093 μm and this decrease in fibre diameter proves that the shell structure was removed. Having the diameter decreased and the fibre structure retained

66

(C) after the shell was dissolved reinforces that the core-shell structure was indeed created.
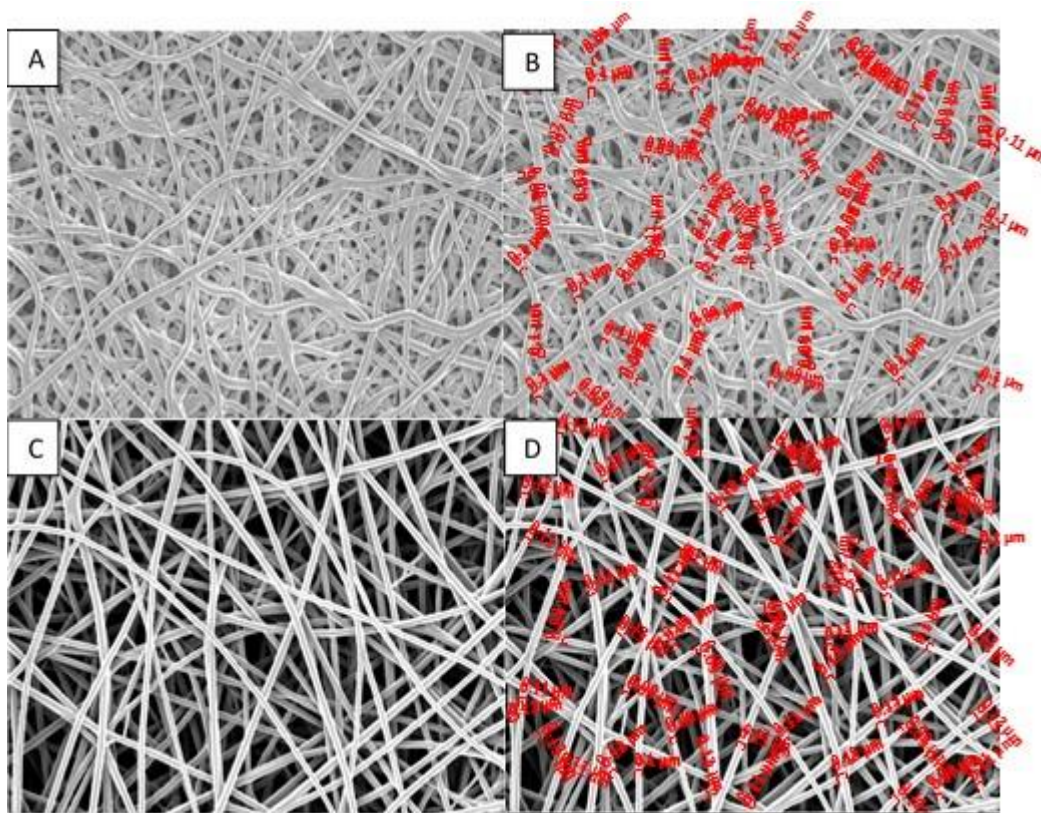

Figure 3.10: SEM images of coaxial fibres (A), the diameter measurement of the coaxial fibres (B), coaxial with the shell dissolved off (C) and the diameter measurements of the dissolved of fibres (D)

Table 3.1: Fibre diameter measurements and standard deviation

	Standard Deviation (µm)	Average fibre Diameter (µm)	Lowest Fibre Diameter (µm)	Highest Fibre Diameter (µm)
Coaxial	0.015	0.111	0.090	0.150
Without the shell	0.010	0.093	0.070	0.110

4.3.2.5 Fluorescence imaging of coaxial fibres

Fluorescence imaging was also used to confirm the coaxial morphology of the nanofibers. To do this, the coaxial samples were tagged with 6-aminofluorescein which

only attaches to the SMI-P and not to nylon 6. This was a good way to determine that the SMI-P (shell polymer) covered the fibres everywhere on the sample. Figure 4.11 shows the coaxial electrospun nanofiber mats. From the images A and B, SMI-P is visible everywhere on the fibres as indicated by the green fluorescence. The SEM images C and D show that the imaged mats had well defined fibres and show a higher resolution of the fibres compared to the fluorescence images. Additionally, the tagged coaxial sample was placed in DMF to dissolve the tagged shell layer and was then imaged. From the fluorescence image E, it can be seen that there is no fluorescence left in the sample, which indicates that the shell was indeed removed from the fibres. However, the fibres could have just been pure SMI-P and SEM imaging was again done on the sample and a complete network of fibres was observed (image F) which again confirmed the core-shell morphology.
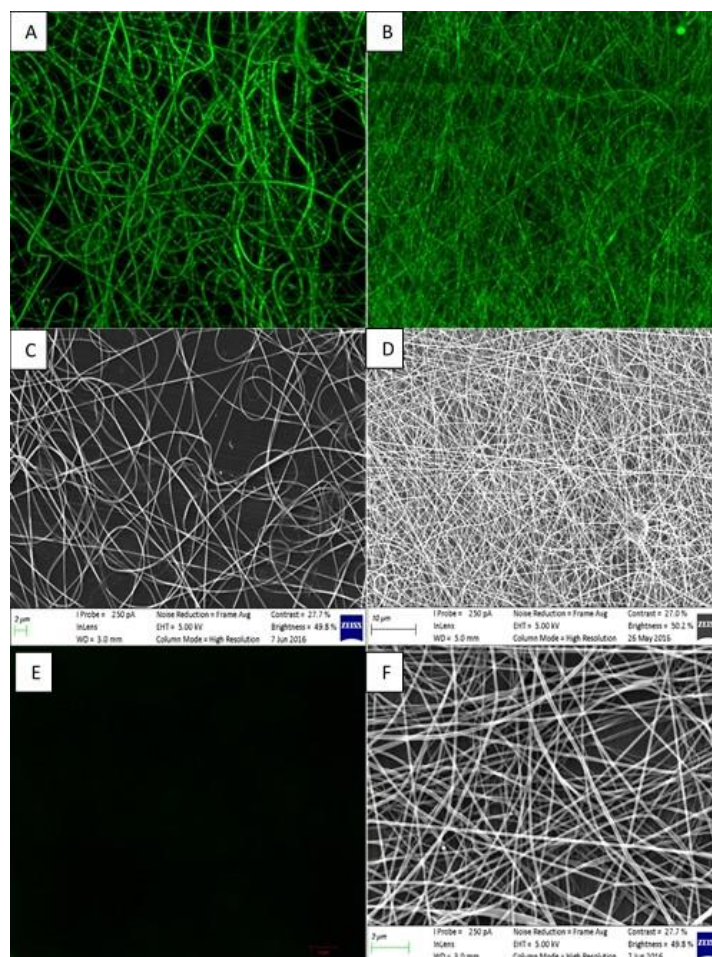

Figure 3.11: Fluorescence images of tagged coaxial fibres (A and B), SEM images of the coaxial nanofibers (C and D), the coaxial fibres with the SMI-P dissolved (F) and the fluorescence image of the coaxial fibres with the SMI-P dissolved (E)

68

4.4   Coaxial fibres obtained via the dip-coating technique

This section reports on the characterization of the coated fibres by FTIR along with the SEM and fluorescence imaging all to provide proof that the nylon 6 fibres were coated.

4.4.1   Modification of the shell polymer for the coating process

This section reports on the characterization of the polymers with lower percentages of converted MAnh and briefly discusses why the lower percentage of MAnh to be converted is required in the coating process.

For the coating process to be successful, some of the highly reactive maleic anhydride moieties had to be available in the polymer to attach to the nylon covalently. Thus, the lower percentage of MAnh to be converted in the SMA allows for the unreacted MAnh to be present in the SMI-P which allows for the covalent bonds with nylon 6 to form. This allows the coating to be bonded to the nylon and the coating is not likely to be removed during use.

4.4.1.1 ATR-FTIR spectroscopy of different percentage SMI-P

In Figure 4.12, the ATR-FTIR spectra of 70% SMI-P (red) and 90% SMI-P (green) are shown. The spectrum is a zoom in on the range of 800 to 2000 cm^{-1} since this is the area that shows the distinction between the polymers. The tertiary amine CN stretch is shown to be more defined as the conversion percentage increased and becomes more like that of fully converted SMI-P as seen in Figure 4.1. The C=O stretch shows an increased intensity as the percentage conversion increases which is expected. The C=O band at 1689 cm^{-1} has 2 peaks unlike that of fully converted SMI-P, but this is due to the shift that occurs from SMA to SMI-P as shown in Figure 4.1, although the band becomes more like the single band of SMI-P as the percentage conversion increases. The bands for the decreasing SMA content do not show up in the spectrum, but this could be affected do to the shift that occurs from SMA to SMI-P thus the split bands are observed instead.
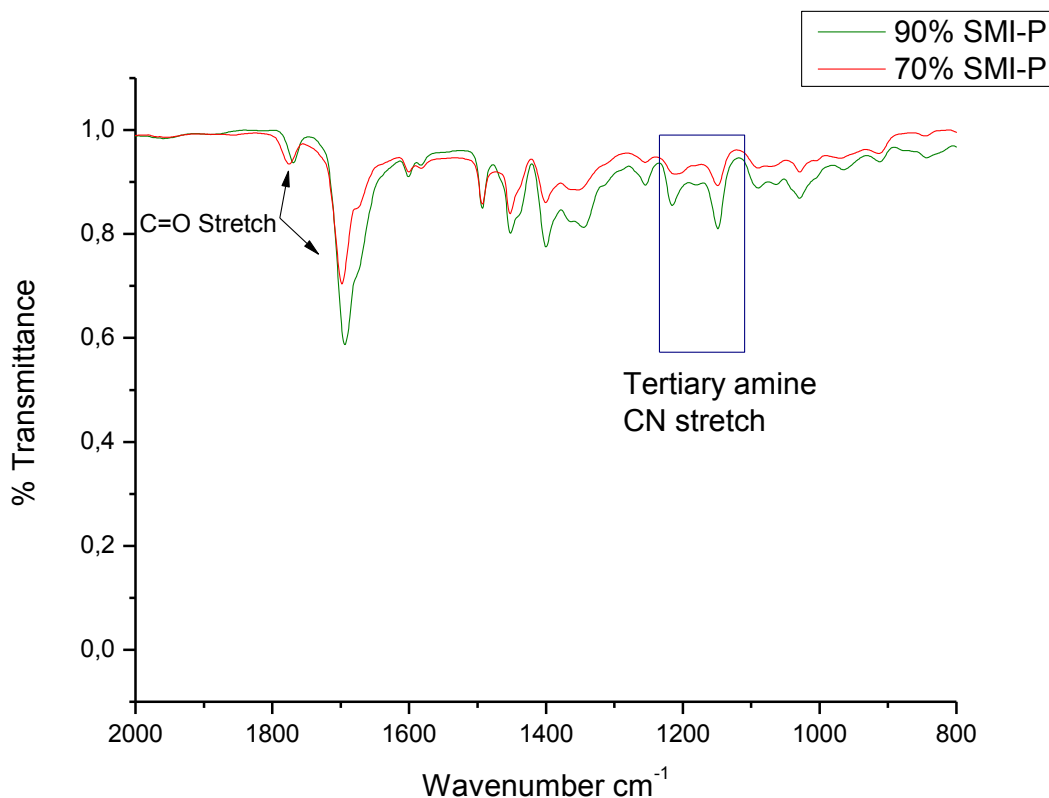
Figure 3.12: ATR–FTIR spectra of 70% and 90% SMI-P

4.4.2   Coated nylon 6

4.4.2.1 ATR-FTIR spectroscopy of coated nylon 6

In Figure 4.13, the ATR-FTIR spectra of the nylon 6 coated nanofibre is shown. The nylon 6 coated with a SMA (A) shows presence of the C=O bands at 1855 and 1770 cm^{-1} which are not present in the pristine nylon 6 sample as shown in Figure 4.4. The presence of the C=O bands proves that SMA is present on the nylon 6 nanofibre mat. Figure 4.13 shows the ATR-FTIR spectra of the nylon 6 coated with 70% SMI-P (B), 90% SMI-P (C) and SMI-P (D). The spectra of B-D show the presence of the different variations of SMI-P by the appearance of the C=O bands at 1770 and 1689 cm^{-1} which is not seen on pristine nylon 6 nanofibre mats and so proves that the SMI-P variations are present on the nylon 6 nanofibre mats.
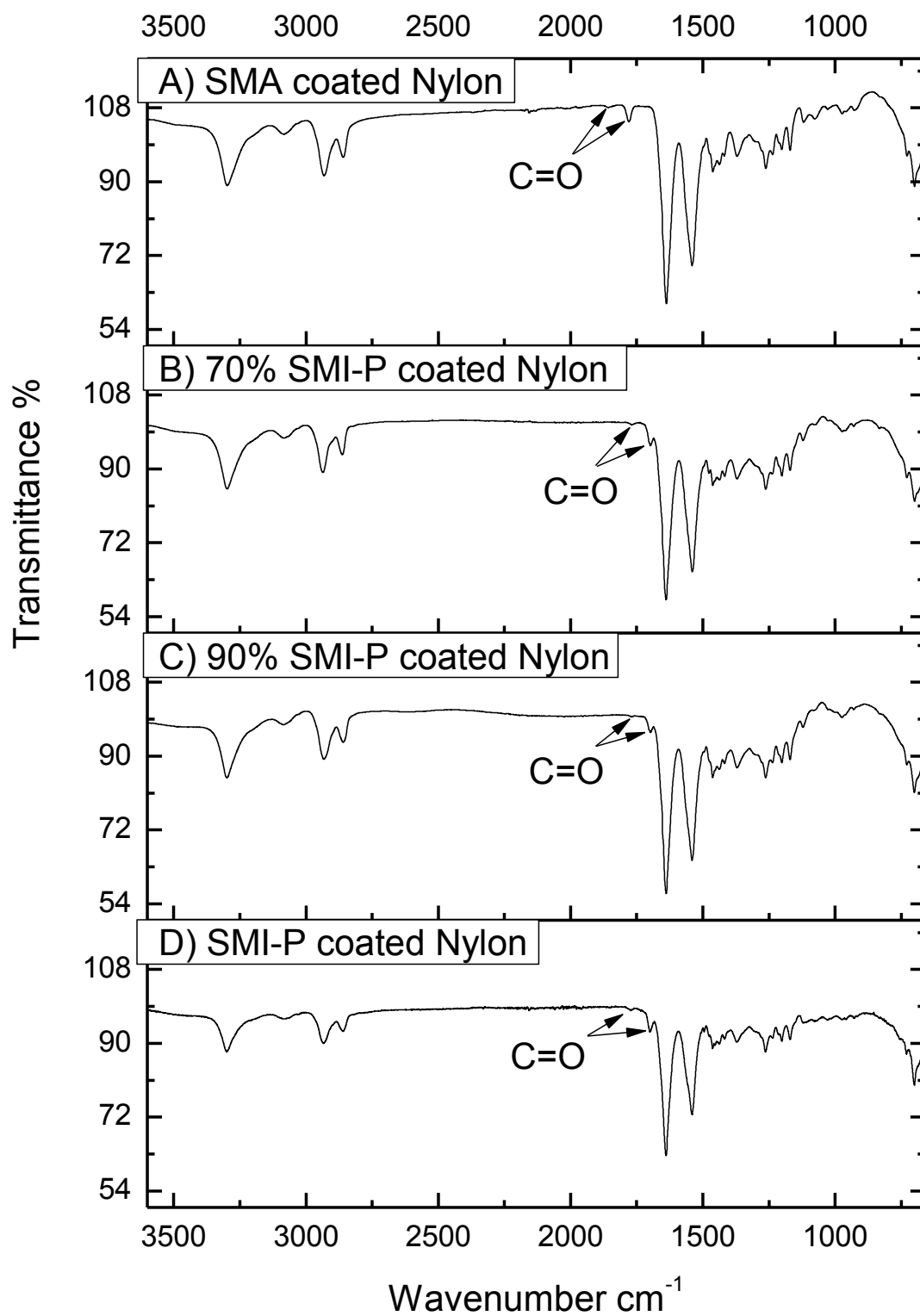
70

Figure 3.13: ATR-FTIR spectra of nylon 6 coated with SMA (A), 70% SMI-P (B), 90% SMI-P (C) and SMI-P (D)

4.4.2.2 Scanning electron microscopy (SEM)

Nylon 6 coated with different variations of SMI-P fibres are shown in Figure 4.14. The images A-D are of the coated nylon 6 fibres that still retained the fibre structure and no films where formed on the fibres as this would inhibit the filtration capabilities of the nanofiber mats. Thus it can be seen that nylon 6 coated with 70% SMI-P (A), 90% SMI-P (B), SMA (C) and SMI-P (D) all still retained the fibre structure and no films where formed over the fibre mats which is what was required.
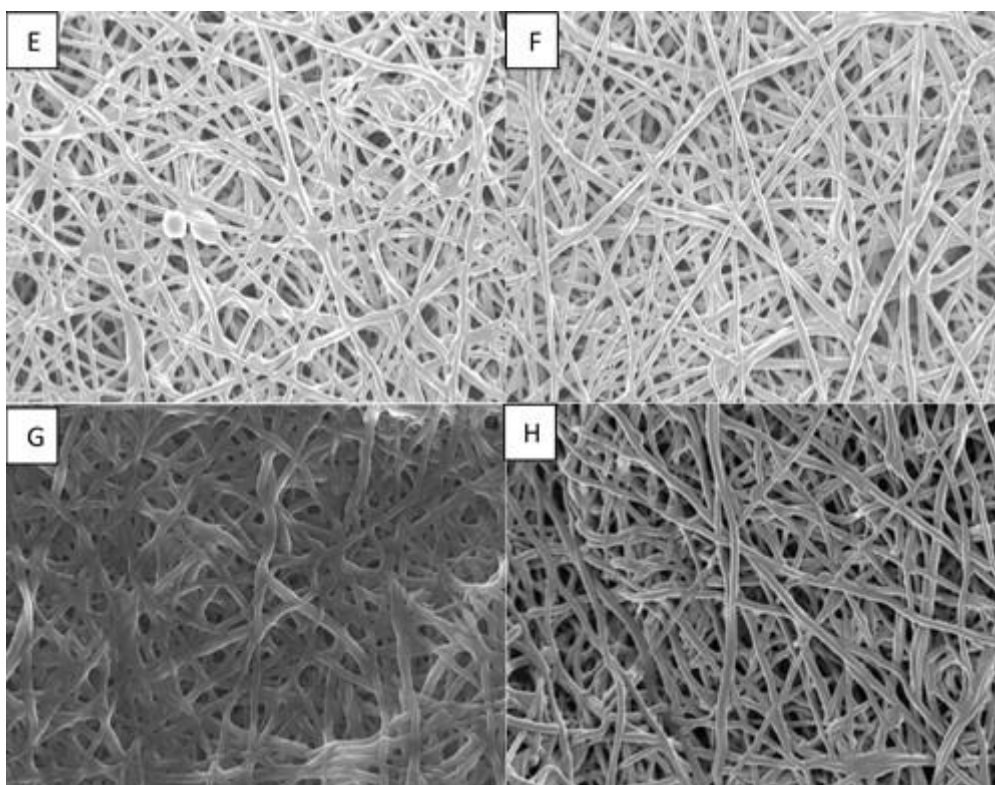

Figure 3.14: SEM images of nylon 6 coated with 70% SMI-P (A), 90% SMI-P (B), SMA (C) and SMI-P (D)

4.5   Fluorescence microscopy of coated nylon 6

A similar procedure as on the fibres fabricated via coaxial electrospinning was followed to confirm the coaxial structure of the nanofibers. Figure 4.15 shows the nylon 6 nanofiber mats that were coated with 70% SMI-P (A and B), 90% SMI-P (C and D) and SMA (E and F). The coatings were tagged with 6 amino fluorescein and were imaged

using confocal microscopy. The samples that fluoresce where coated by 70% SMI-P (A), 90% SMI-P (C) and SMA (E). The samples also show the fibre structure still being retained and no films were formed from the coating process. Thus, with the ATR-FTIR images (Figures 4.7 - 4.9) and the fluorescing images in Figure 4.15 it can be successfully being concluded that the coating process was successful.
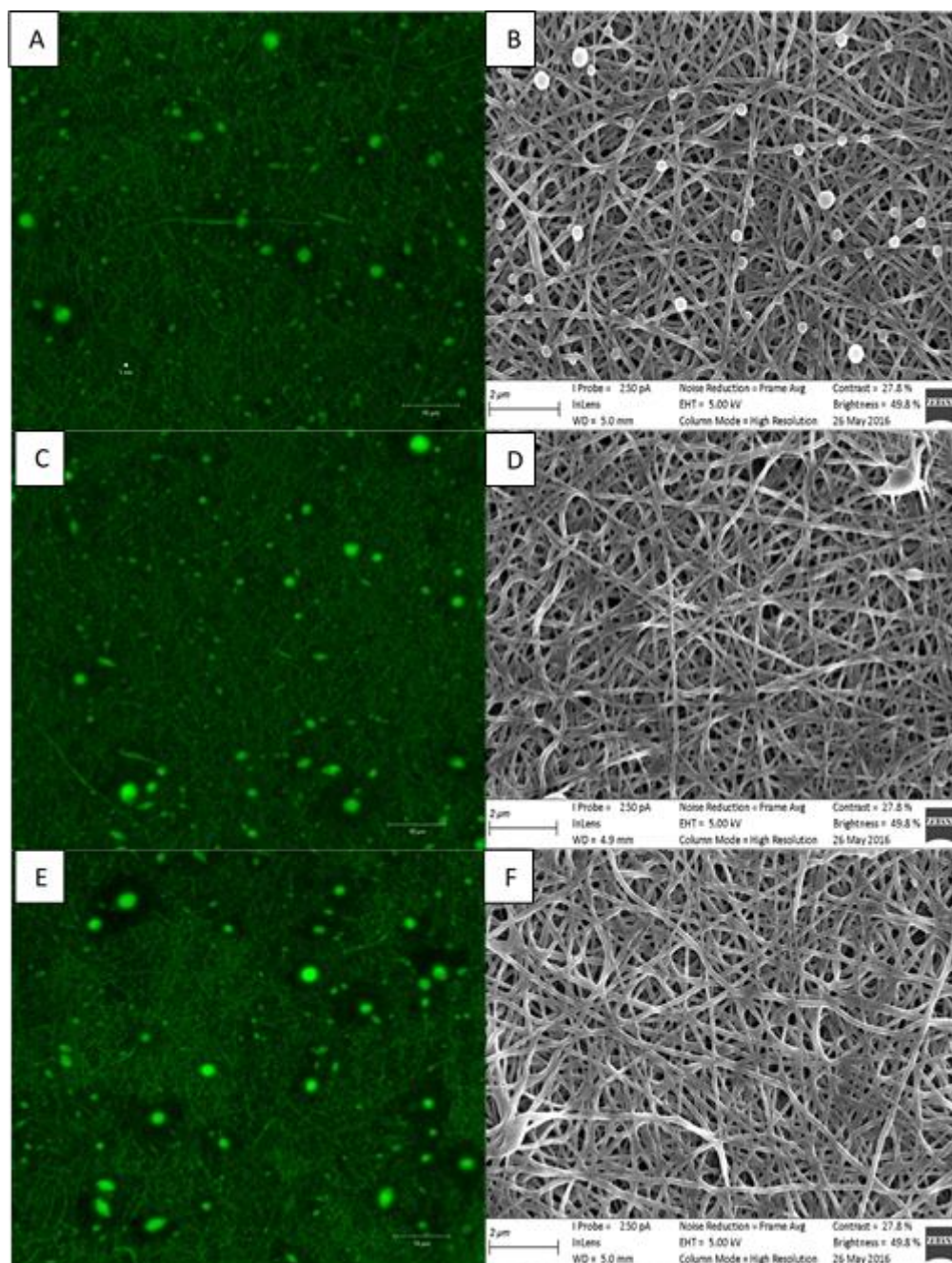

Figure 3.15: Fluorescence and SEM images of 70% SMI-P (A, B), 90% SMI-P (C, D), SMA (E, F)

73

Figure 4.16 shows the nylon 6 nanofiber mats that were coated with 70% SMI-P (H), 90% SMI-P (J) and SMA (L) after the samples were placed in water for a week. The samples were placed in water in order to see if water has any effect on the coating as the fibre mats has a possible end use in water filtration. The coatings were tagged with 6 amino fluorescein and were imaged using confocal microscopy. Samples G, I and K are the fluorescence images of the samples that where left in water for a week and these show that the coatings are still present. Thus it can be seen that being in the presence of water the coatings are not removed from the samples or damaged.
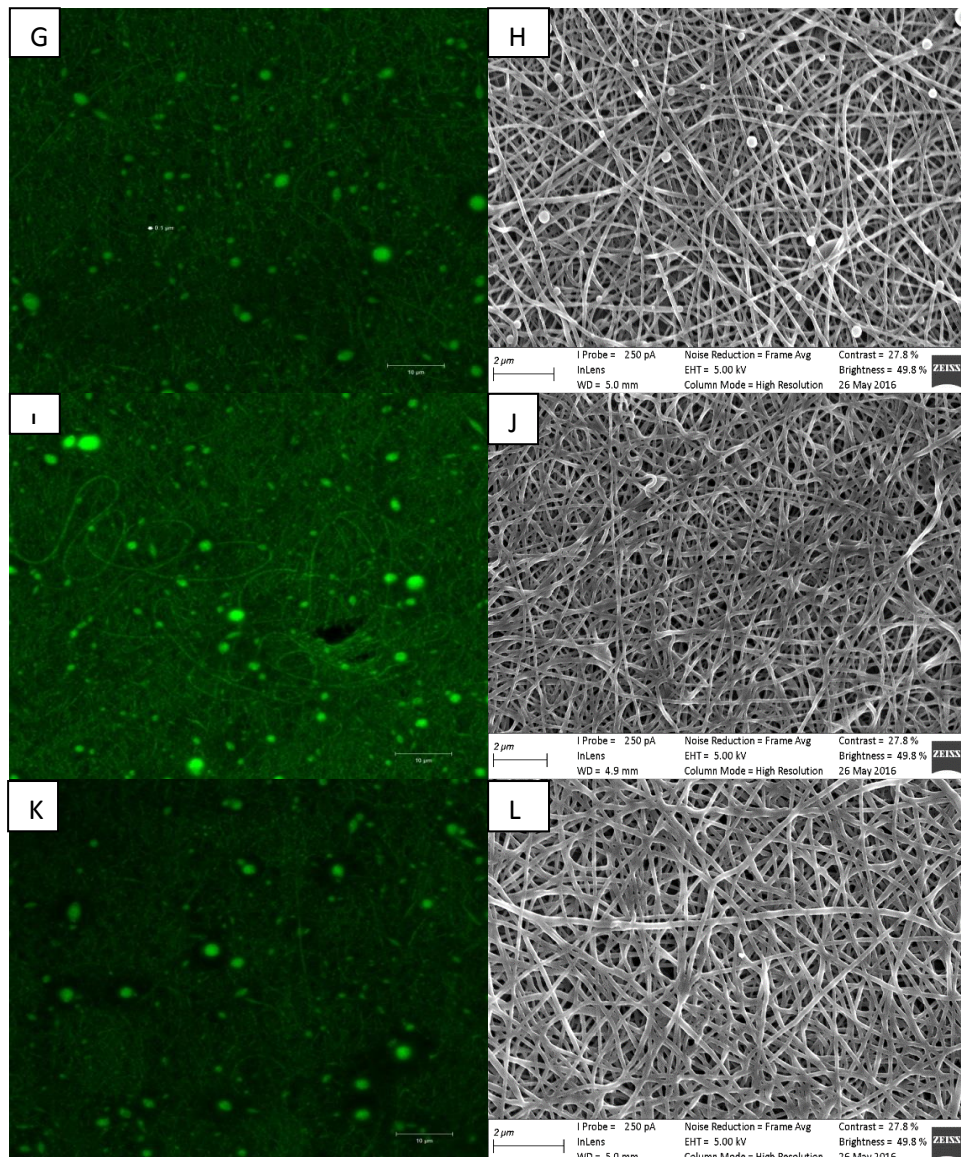

Figure 3.16: Fluorescence and SEM images of 70% SMI-P (G, H), 90% SMI-P (I, J), SMA (K, L) after being in water for a week

4.6   Antimicrobial characterization

This section reports on the antimicrobial activity of the produced nanofibers since one of the aims was to observe if the polymers retain their antimicrobial activity that they possessed before the reinforcement was applied. This was done by two methods which were the zone inhibition tests and the fluorescence live/dead tests. These tests were carried out as discussed in Section 3.9.

4.6.1   Zone inhibition tests

4.6.1.1 Antimicrobial results on the electrospun fibres

Figure 4.17 shows the results of the electrospun fibres and the controls treated with *E. coli,* as an example of what was observed from the zone inhibition tests. The nylon 6 nanofibre mat and the nylon 6 nanofibre mat coated with SMA are shown in Figure 4.17 (1). The samples in (1) shows that there is no antimicrobial activity which is expected since these samples have no antimicrobial properties and were used as the controls for the zone inanition tests. The sample in Figure 4.17 (2) A shows a control with no antimicrobial polymers present. The results shown by (2) in Figure 4.17 show that SMI-P (B), 90 % SMI-P (C) and 70% SMI-P (D) possess antimicrobial activity as evidenced by the clearing around the samples. The clearings around the samples were very inconsistent and so the diameters were not measured, but the results of the test were reported as positive or negative depending whether the samples show antimicrobial activity or not. These results are reported in Table 4.2. The test indicated that the samples had antimicrobial activity against all the bacteria tested, but the amount of activity varied as shown in Table 4.2. Due to time constraints, only two bacteria were used for further testing and it was decided to use both a gram positive and a gram negative bacteria strain against which the samples showed high antimicrobial activity. Thus, it was decided to perform the tests in Section 4.6.2 on *Staphylococcus aureus* and *Pseudomonas aeruginosa.*
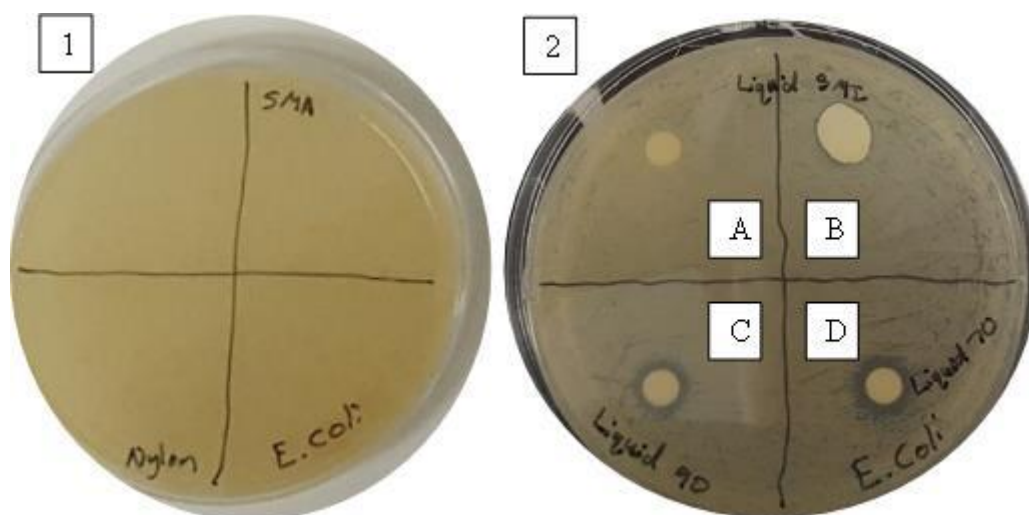
Figure 3.17: Nylon 6 nanofibre mat (1), nylon 6 nanofibre mat coated with SMA (1), Control(2A), SMI-P (2B), 90% SMI-P (2C) and 70% SMI-P(2D) treated with *E. coli*

Table 0.2: Antimicrobial assay results of the zone inhibition tests

Gram status	Bacteria strain	Activity
+	*Staphylococcus aureus*	Positive (highly)
-	*Salmonella typhi*	Positive (Low - moderate)
-	*Pseudomonas aeruginosa*	Positive (highly)
-	*Escherichia coli*	Positive (highly)
+	*Methicillin resistant Staphylococcus aureus*	Positive (Low – moderate)
+	*Bacillus subtilis*	Positive (Low - moderate)

4.6.2   Live/Dead fluorescence method

Figure 4.18 shows the results of the live/dead bacteria test with *S. aureus*. For this test, the samples were exposed to the bacteria 15 minutes prior to the imaging. The samples were also imaged after 24 hours exposure. From the images of nylon 6 nanofiber mats coated with 70% SMI-P (A), 90% SMI-P (C), SMI-P (E) and the coaxial nanofiber mats (G) show that the bacteria were alive and the images 24 hours later of nylon 6 nanofiber mats coated with 70% SMI-P (B), 90% SMI-P (D), SMI-P (F) and the coaxial nanofiber mats (H) show that all the bacteria that were added to the samples had died. The result of

this test is exactly what was expected as all the mentioned samples possess antimicrobial properties.
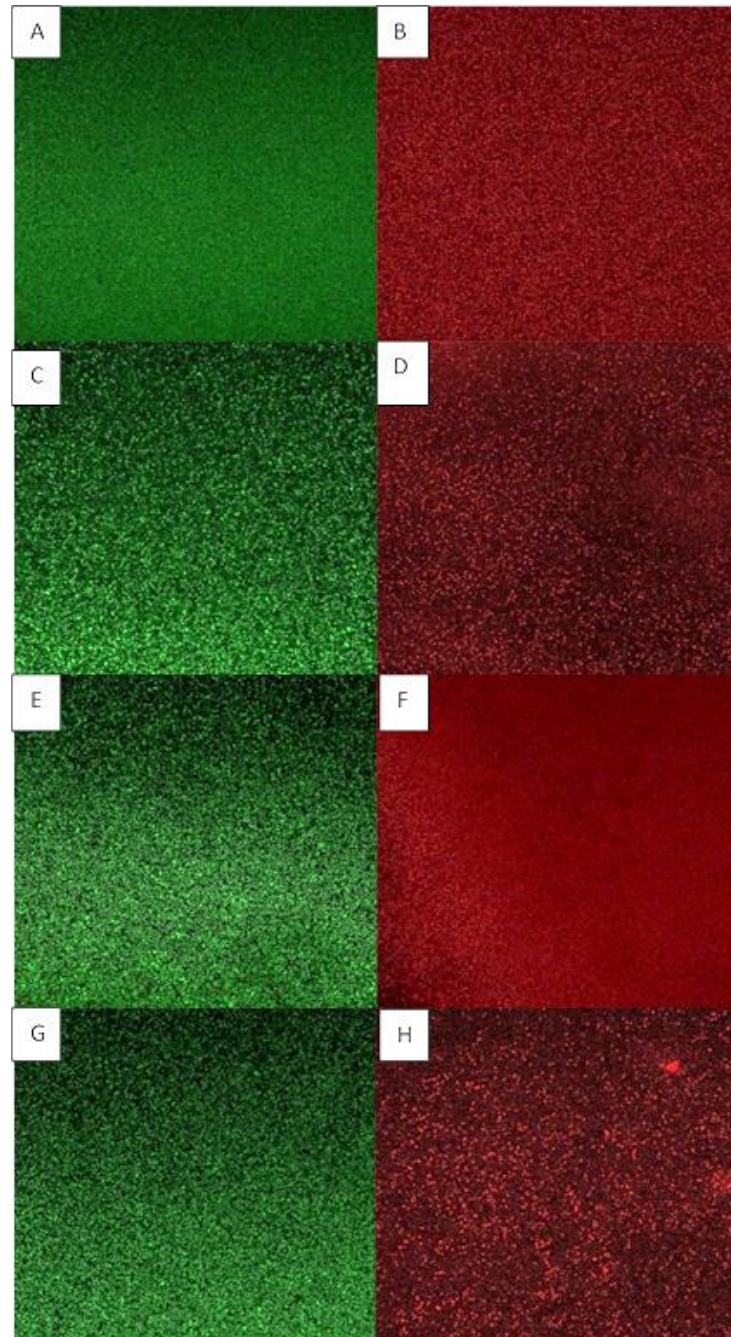

Figure 3.18: Fluorescence images after 15 minutes of nylon 6 nanofiber mats coated with 70% SMI-P (A), 90% SMI-P (C), SMI-P (E) and the coaxial nanofiber mats (G) and the images after 24 hours of nylon 6 nanofiber mats coated with 70% SMI-P (B), 90% SMI-P (D), SMI-P (F) and the coaxial nanofiber mats (H) that was treated with *S. aureus* bacterium

Figure 4.19 shows the results of the live/dead bacteria test with *S. aureus* which was done by taking fluorescence images around 15 minutes after the bacteria were added to the samples and then the samples where imaged again after 24 hours. Thus, the images of nylon 6 (I), nylon 6 coated with SMA (K), nylon 6 coated with SMA after which the SMA was modified to SMI-P (M) and SMI-P (O) nanofibers show that the bacteria were alive. The images 24 hours later of nylon 6 (J), nylon 6 coated with SMA (L), nylon 6 coated with SMA and then modified to SMI-P (N) and SMI-P (P) nanofibers show that all the bacteria had died except for I and L which still had all the bacteria alive. The result of this test is exactly what was expected as all the mentioned samples except for (I, J, K, L) had antimicrobial properties.
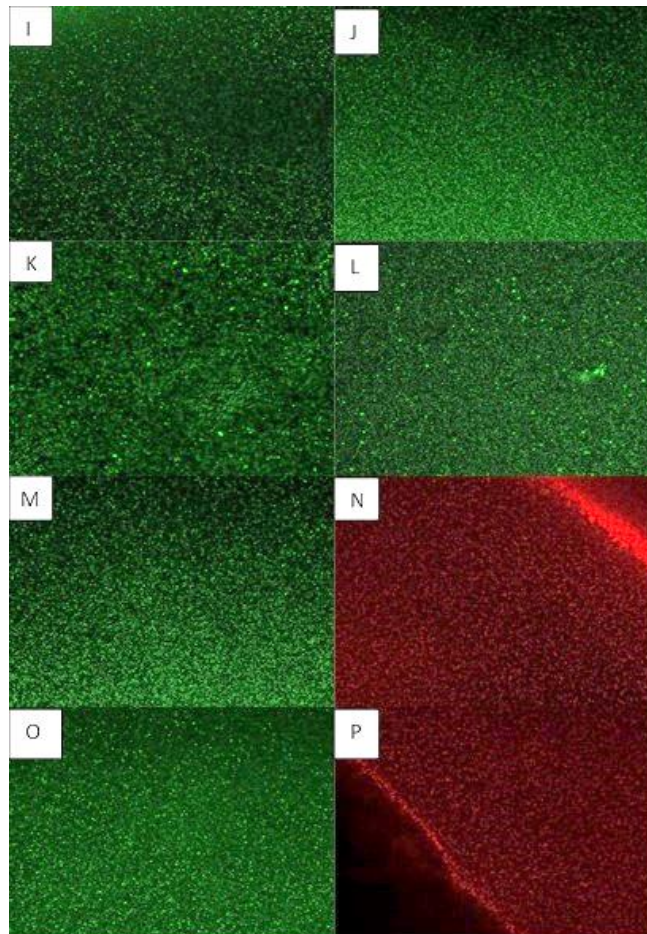

Figure 3.19: Fluorescence images after 15 minutes of nylon 6 (I), SMI-P (O) nanofibers, nylon 6 coated with SMA (K), nylon 6 Coated with SMA, then converted to SMI-P (M) and the images after 24 hours of nylon 6 (J), SMI-P (P) nanofibers, nylon 6 coated with SMA (L), nylon 6 Coated with SMA, then converted to SMI-P (N) that was treated with *S. aureus* bacterium

Figure 4.20 shows the results of the live/dead bacteria test with *P. aeruginosa* which was done by taking fluorescence images around 15 minutes after the bacteria were added to the samples and then the samples where imaged again after 2 hours which was determined to be roughly the time it took to kill all the bacteria. Thus, the images of nylon 6 nanofiber mats coated with 70% SMI-P (A), 90% SMI-P (C), SMI-P (E) and the coaxial nanofiber mats (G) show that the bacteria were alive and the images 2 hours later of nylon 6 nanofiber mats coated with 70% SMI-P (B), 90% SMI-P (D), SMI-P (F) and the coaxial nanofiber mats (H) show that all the bacteria that were added to the samples has died. The result of this test is exactly what was expected as all the mentioned samples possess antimicrobial properties
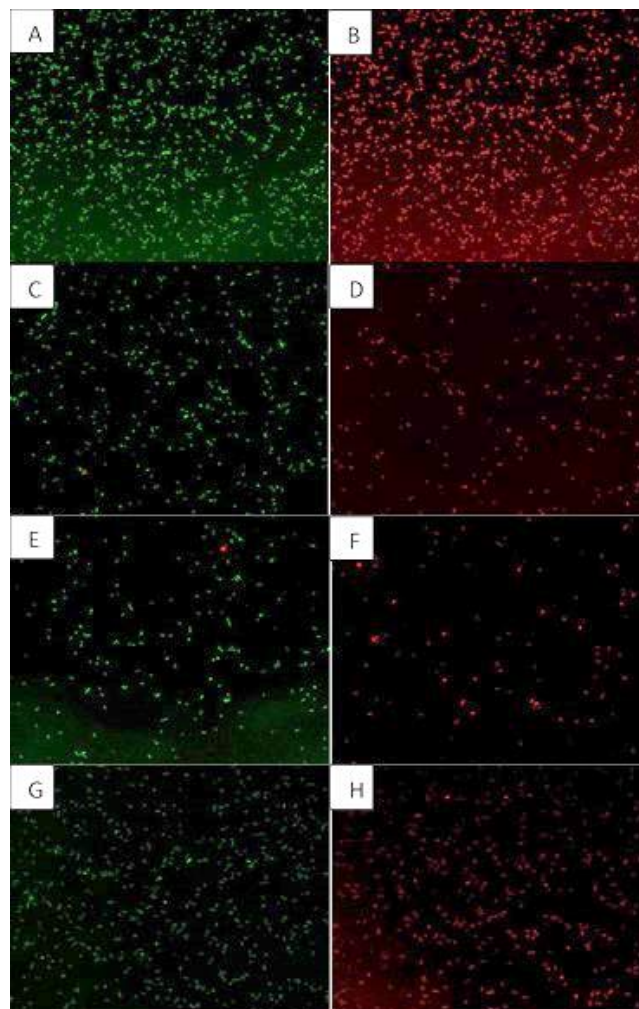

Figure 3.20: Fluorescence images of nylon 6 nanofiber mats coated with 70% SMI-P (A after 15 minutes, B after 2 hours), 90% SMI-P (C after 15 minutes, D after 2 hours), SMI-P (E after 15 minutes, F after 2 hours) and the coaxial nanofiber mats (G after 15 minutes, H after 2 hours) that where treated with *P. aeruginosa* bacterium

Figure 4.21 shows the results of the live/dead bacteria test with *P. aeruginosa* which was done by taking fluorescence images around 15 minutes after the bacteria were added to the samples and then the samples where imaged again after 2 hours which was determined to be roughly the time it took to kill all the bacteria. Thus, the images of nylon 6 (I), SMI-P (O) nanofibers, nylon 6 coated with SMA (K) and nylon 6 coated with SMA and then converted to SMI-P (M) show that the bacteria were alive and the images 24 hours later of nylon 6 (J), SMI-P (P) nanofibers, nylon 6 coated with SMA (L) and nylon 6 coated with SMA and then converted to SMI-P (N) show that all the bacteria that were added to the samples had died except for I and L which still had all the bacteria alive. The result of this test is exactly what was expected as all the mentioned samples except for (I, J, K, L) had antimicrobial properties.
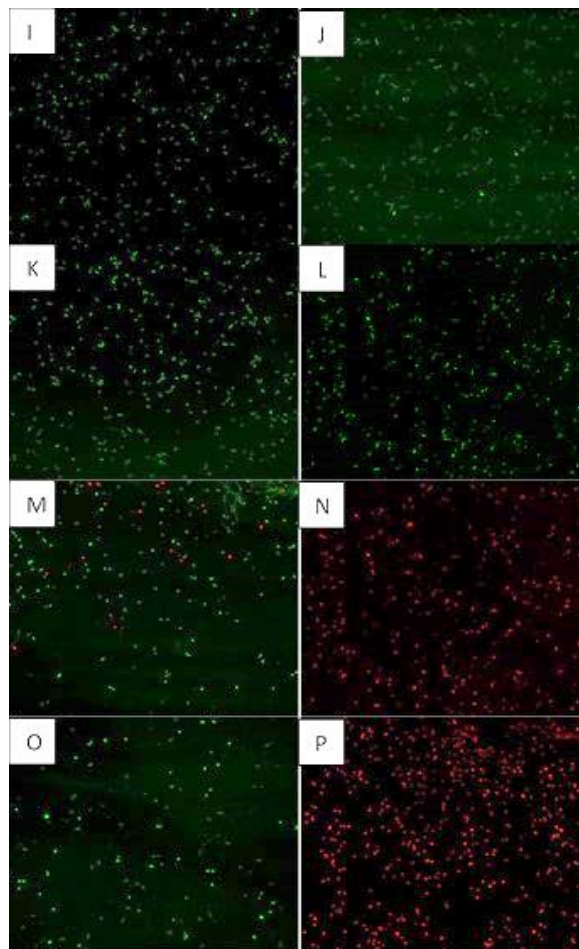

Figure 3.21: Fluorescence images of nylon 6 (I after 15 minutes, J after 2 hours), SMI-P (O after 15 minutes, P after 2 hours) nanofibers, nylon 6 coated with SMA (K after 15 minutes, L after 2 hours) and nylon 6 Coated with SMA and then converted to SMI-P (M after 15 minutes, N after 2 hours) that is treated with *P. aeruginosa* bacterium

4.7   Mechanical tests

The tensile strength of the fibres was initially meant to be tested using an Instron tensile tester, but it was found that the tensile strength of the samples was not high enough to have the data recorded by the equipment. The fibres were even aligned using a drum collector instead of the standard collector, but even this was not enough to allow for a reading on the Instron equipment. Thus, the tensile strength was tested by hand in the lab where the samples were pulled apart. The use of this simple tensile strength test showed a clear increase in tensile strength of the samples after nylon 6 was incorporated as this required a little effort to break whereas the pure SMI-P fibres literally just pulled apart with very little to no resistance. Thus, it can be said that the coaxial fibres and the nylon 6 coated fibres have a higher tensile strength compared the pure SMI-P.

4.7.1   Abrasion tests

The abrasion tests were tested manually without any instruments and SEM was carried out on the fibres after the abrasion tests were performed. Figure 4.22 shows the SEM images of the samples after the abrasion tests were carried out. The SEM images of nylon 6 coated with 70% SMI-P (A), 90% SMI-P (B), SM-P (C), SMA that was modified to SMI-P (D) and SMA (E) showed that after the abrasion test the fibres were still intact. Then the images of nylon 6 (F) and coaxial (G) nanofibers also show that after the abrasion test the fibres were still intact. Then the SEM image of pristine SMI-P (H) after the abrasion test showed that the fibres ended up breaking due to the test and so this shows that the addition of nylon 6 as a reinforcement polymer allowed for the strengthening of the core-shell nanofibres as seen from the abrasion tests. The abrasion tests on the pristine SMI-P nanofibre mats were very difficult as the sample just tends to break apart as the test was performed, but the SEM image was performed on a piece of the sample that was not destroyed. The abrasion tests were performed by rubbing the sample back and forth 5 times using one's finger. This was repeated for all the samples.
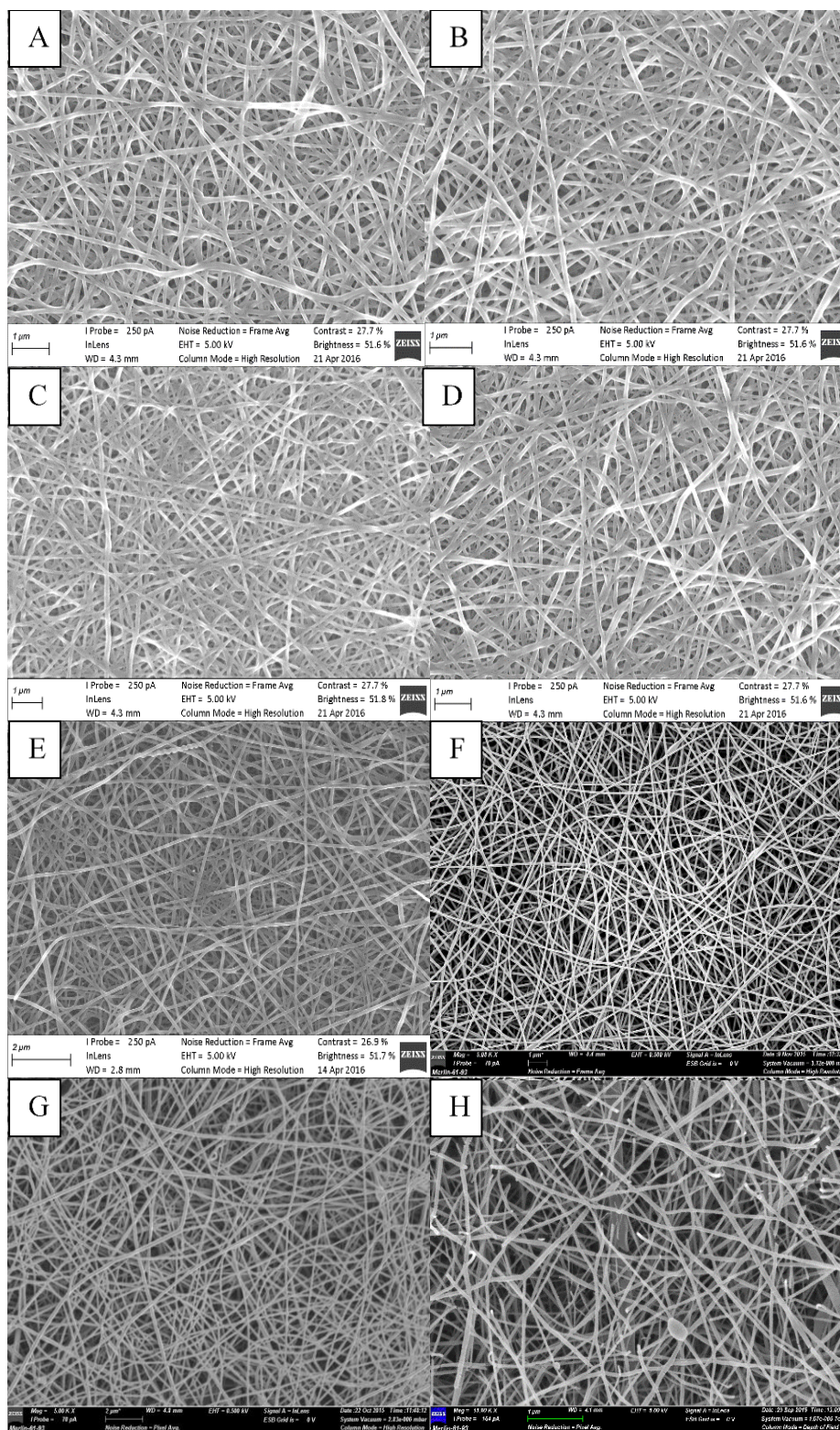
Figure 3.22: The SEM images of nylon 6 nanofibre mats coated with 70% SMI-P (A), 90% SMI-P (B), SM-P (C), SMA that was modified to SMI-P (D), SMA (E) and nylon 6 (F), coaxial (G) as well as SMI-P (H) nanofibre mats after the abrasion tests

4.8   References

1.   Bshena, O. E. S. Synthesis of permanent non-leaching antimicrobial polymer nanofibers. University of Stellenbosch, Stellenbosch, 2012. PhD

2.   Cronje, L. Surface modification of styrene maleic anhydride nanofibers for efficient capture of Mycobacterium tuberculosis. Stellenbosch University, Stellenbosch, 2012. PhD

3.   Zarrini, K.; Rahimi, A. A.; Alihosseini, F.; Fashandi, H., Highly efficient dye adsorbent based on polyaniline-coated nylon-6 nanofibers. *Journal of Cleaner Production* **2016,** *30*, 1-10.

4.   Kagan, V. A., Advantages of welded nylon for powertrain application: linear vibration, orbital and hot-plate joining Technologies. *New Materials & Development Processes* **1999,** *1*, 65-75.

CHAPTER 5

Conclusions and recommendations

This chapter reports on how the objectives set in Section 1.4 were met and the recommendations for possible further studies.

5.1   Conclusions

SMI-P and its variants were successfully synthesised and characterised for use in this study. The coaxial electrospinning setup was made with commercially available materials. The polymer solutions used for the core and shell were delivered to the spinneret in a reproducible and controlled manner. Coaxial nanofibers were made via two techniques which are electrospinning and dip coating. The core-shell structure was confirmed via scanning transmission electron microscopy (STEM) and fluorescence microscopy. The addition of uranyl acetate in the core solution during the coaxial electrospinning allowed for the visualization of the core-shell structure using STEM as shown in Section 4.2. Additional tests such as the dissolution tests allowed for the further proof that the core-shell structure was produced. Additionally, FTIR and DSC analysis also built on added proof that the core-shell fibres were produced.

The fibre mats produced by the two methods were tested in order to determine whether the fibres gained tensile strength and this was done by a physical abrasion test performed by the investigator of this study. The tensile test results showed that both the coaxial electrospun and the coated nylon 6 fibres increased in tensile strength when compared to pristine SMI-P.

The antimicrobial activity of all the synthesized coaxial polymer fibres produced in this study was successfully tested as shown in Section 4.5. The results showed that the coaxial fibres along with the coated nylon 6 fibres all retained the antimicrobial activity that pristine SMI-P possessed.

Thus, from this study, novel strengthened SMI-P nanofiber mats were produced and can be used for many applications including water filtration and some medical applications.

The strengthened SMI-P will most likely last longer than pristine SMI-P fibre mats without having a negative effect on the antimicrobial activity.

5.2   Recommendations

For future research, it can be considered to try different reinforcement polymers to produce other reinforced samples. It can also be considered to perform different antimicrobial tests in order to gain results that can be compared in order to find out what percentage of the original antimicrobial activity of SMI-P was retained by the new reinforced samples. This study can also be reproduced for other antimicrobial polymers that may require reinforcement for their end uses.